HHS Public Access

Author manuscript

Nat Immunol. Author manuscript; available in PMC 2014 April 01.

Published in final edited form as:

Nat Immunol. 2013 October ; 14(10): 1084–1092. doi:10.1038/ni.2688.

MEF2B mutations lead to deregulated expression of the *BCL6* oncogene in Diffuse Large B cell Lymphoma

Carol Y. Ying[1], **David Dominguez-Sola**[1], **Melissa Fabi**[1], **Ivo C. Lorenz**[1,^], **Shafinaz Hussein**[1,2], **Mukesh Bansal**[3], **Andrea Califano**[1,3,4], **Laura Pasqualucci**[1,2,4], **Katia Basso**[1,2], and **Riccardo Dalla-Favera**[1,2,4,5,6,*]

[1]Institute for Cancer Genetics, Columbia University, New York, NY 10032, USA

[2]Department of Pathology and Cell Biology, Columbia University, New York, NY 10032, USA

[3]Joint Centers for Systems Biology, Columbia University, New York, NY 10032, USA

[4]Herbert Irving Comprehensive Cancer Center, Columbia University, New York, NY 10032, USA

[5]Department of Genetics and Development, Columbia University, New York, NY 10032, USA

[6]Department of Microbiology and Immunology, Columbia University, New York, NY 10032, USA

Abstract

The *MEF2B* gene encodes a transcriptional activator and is found mutated in ∼11% of diffuse large B cell lymphomas (DLBCLs) and ∼12% of follicular lymphomas. Here, we show that MEF2B directly activates the transcription of the proto-oncogene *BCL6* in normal germinal-center B cells and is required for DLBCL proliferation. *MEF2B* mutations enhance MEF2B transcriptional activity either by disrupting its interaction with the co-repressor CABIN1, or by rendering it insensitive to phosphorylation- and sumoylation-mediated inhibitory signaling events. Consequently, Bcl-6 transcriptional activity is deregulated in DLBCL harboring *MEF2B* mutations. Thus, somatic mutations of *MEF2B* may contribute to lymphomagenesis by deregulating the expression of the *BCL6* oncogene, and MEF2B may represent an alternative target to block Bcl-6 activity in DLBCLs.

*Correspondence: rd10@columbia.edu (R.D.-F.).

^Present address: Boehringer Ingelheim Pharmaceuticals, Inc, Ridgefield, CT 06877

AUTHOR CONTRIBUTIONS

C.Y.Y. and R.D.-F. designed the study and wrote the manuscript. C.Y.Y. conducted experiments and analyzed data. D.D.S. performed and contributed to the design and execution of the experiments and data analysis. M.F. performed co-immunoprecipitation assay. I.C.L. performed structural analysis. S.H. contributed to the immunofluorescence staining. M.B. performed bioinformatics analysis, which was supervised by A.C. L.P. conducted and supervised genomic analysis. K.B. contributed to the original design of the study. D.D.S., K.B., L.P., and I.C.L. edited the manuscript. All authors read and approved the manuscript.

Competing Financial Interests

The authors declare no competing financial interests.

INTRODUCTION

Diffuse large B cell lymphoma (DLBCL) is the most common form of non-Hodgkin's lymphoma in adults, accounting for approximately 40% of diagnoses and also arising from transformation of follicular lymphoma (FL)[1]. Gene expression profiling studies identified the heterogeneity of this germinal center (GC)-related malignancy by distinguishing three phenotypic subtypes, namely germinal center B cell-like (GCB) DLBCL, activated B cell-like (ABC) DLBCL and primary mediastinal B cell lymphoma (PMBL)[2], with a small subset of cases that remain unclassified. These subtypes differ in their genotype, phenotype and notably, clinical features, including differential response to the currently adopted immunochemotherapy-based regimen[3]. Although a subset of DLBCL patients can be cured, a substantial fraction of them (~40%) die of the disease[3], indicating the need to develop more specific targeted therapies.

Recent technological advances, including whole-genome DNA and RNA sequencing and genome-wide copy-number analysis, have provided a comprehensive view of the genomic landscape of GCB- and ABC-DLBCLs, allowing new insights in the genetic lesions associated with the pathogenesis of this malignancy[4–7]. These approaches have identified a number of recurrent lesions that are present in both subtypes of DLBCL, including those involving chromatin acetylation and methylation functions, alterations that deregulate the GC master regulator Bcl-6 and those leading to immune escape[4,5,8–10]. In addition, these studies have confirmed or newly identified genetic lesions preferentially associated with GCB DLBCLs, including chromosomal translocations involving *MYC* and *BCL2*, and mutational activation of the chromatin remodeling gene *EZH2*, as well as lesions preferentially associated with ABC DLBCL, including those leading to activation of the transcription complex NF-κB, translocations involving *BCL6* and mutational inactivation of the master regulator of plasma cell differentiation *PRDM1*[10–16].

Among the genetic alterations recurrently found in DLBCL and FL, but remaining of unclear functional relevance, are mutations affecting the *MEF2B* gene[4–7]. MEF2B is a member of the myocyte enhancer-binding factor 2 (MEF2) family of transcription factors (including MEF2A, -B, -C, -D), which are characterized by high homology in the MADS (MCM1 Agamous Deficiens SRF) box and an adjacent MEF2 domain[17]. Together, these two conserved domains in the N-terminal half of MEF2B direct DNA binding, homodimerization of MEF2 polypeptides and interaction with specific transcriptional co-factors. The highly divergent C-terminal half of MEF2 proteins has been suggested to modulate their transcriptional activity[17,18]. The spectrum of targets activated by MEF2 transcription factors in different cell types is dependent on association with specific co-repressors and co-activators in response to multiple signaling pathways[17]. In particular, MEF2B functions as a transcriptional activator by binding to specific A/T rich DNA sequences originally identified in the control regions of muscle-specific and growth factor-related genes[18,19]. Its activity is regulated by the alternative binding of either the CABIN1 co-repressor or class II histone deacetylases (HDACs) to its N-terminus depending on the specific cellular context[20,21]. The *MEF2B* gene can express at least two protein isoforms (A and B), which carry distinct C-terminal domains. In addition, several transcripts, some of which are tissue specific, are generated via alternative splicing. In lymphocytes, a MEF2

family member, MEF2D, is involved in T cell receptor-mediated apoptosis and the response to calcium signaling in thymocytes[21,22], while MEF2C is required for the formation of the GC[23,24]. In the present study, we identified the functional consequences of the genetic alterations affecting *MEF2B* in DLBCLs and FLs, and reveal a new role for MEF2B as a master regulator of the GC gene *BCL6*.

RESULTS

MEF2B gene mutations in DLBCL and FL

To further investigate the mutations affecting *MEF2B* in DLBCL and FL, we extended our previous analysis[4] to include a total of 134 DLBCL samples (111 primary cases and 23 cell lines), as well as 35 FL primary cases (Fig. 1). Using genomic PCR amplification and Sanger sequencing of the *MEF2B* coding region, we identified 11 sequence variants, distributed in 10/134 DLBCL cases and 1/35 FL cases (Supplementary Table 1). The somatic origin of the mutations was confirmed by analysis of paired normal DNA, available in 3 cases from either our own panel or other reported data sets[5,6]. The expression of the *MEF2B* mutant alleles was verified in DLBCL primary cases, and the heterozygous nature of the mutations was confirmed in all mutated DLBCL cell lines. With the exception of a frameshift deletion, all *MEF2B* mutations affected the two known isoforms (A and B) of MEF2B, both of which are expressed in B cells (Supplementary Table 1, Supplementary Fig. 1).

Considering also the mutations reported by three other studies[5–7], most observed variants are missense mutations (69%, 27/39), while eight frameshift and four nonsense mutations account for the remainder (Fig. 1a). Most missense mutations (85%) are clustered in the region encoding the N-terminal conserved MADS-box and MEF2 functional domains, suggesting that they may have an impact on MEF2B transcriptional function (Fig. 1a). In this region, six amino acid changes of confirmed somatic origin (K4E, K5N, Y69H, E77K, N81Y, D83V), recurrently affected the same codons in distinct DLBCL and FL cases (Fig. 1a).

While 81% (73/90) of all reported *MEF2B*-mutated cases have alterations affecting the N-terminal region of MEF2B, a second group of cases (19%, 17/90) carried *MEF2B* mutations that affect the C-terminal half of the protein, and included a mixture of frameshift, missense and nonsense mutations, and no recurrent events (Fig. 1a). The nonsense mutations and the majority of frameshift mutations were predicted to generate truncated proteins by deleting different lengths of the C-terminus. Two of these alleles (R171X and Y201X) express C-terminal truncated forms of MEF2B protein of ∼19 kDa and ∼22 kDa, respectively, while the frameshift mutations (G242fs, P256fs, and L269fs), when expressed in mRNAs encoding for isoform A, are predicted to generate a full-length protein similar to wild-type isoform B, except for a unique stretch of inserted amino acids (Supplementary Fig. 1). Collectively, these alleles encode proteins with C-terminal truncations or mimicking the wild-type MEF2B isoform B, which carries a distinct C-terminus (Supplementary Fig. 1).

In conclusion, *MEF2B* was found mutated in 7.5% of DLBCL cases in our panel, including both GCB (7/66, 10.6%) and ABC (3/68, 4.4%) subtypes, and in 3% of FL cases (1/35) (Fig. 1b).

MEF2B expression is induced in germinal center B cells

We investigated the expression pattern of *MEF2B* in normal mature B cell subpopulations isolated from human tonsils[25]. *MEF2B* RNA, but not that of other members of the MEF2 family, was abundantly expressed in GC B cells, with low expression in naive and memory B cells (Fig. 2a). The expression pattern of *MEF2B* transcripts in these B cell subpopulations is similar to that of the proto-oncogene *BCL6* (Fig. 2a,b), which encodes a transcription factor selectively expressed in GC B cells within the mature B cell lineage, is required for GC formation, and whose deregulated expression is implicated in lymphomagenesis[26,27]. Transcripts corresponding to both A and B isoforms of *MEF2B* were detected in GC B cells (data not shown), and MEF2B protein expression was high in GC B cells, while it was absent in naive B cells and follicular mantle zones (Fig. 2c,d). The association of MEF2B expression with the GC B cell fate was further confirmed in secondary lymphoid tissues of mice challenged with T cell-dependent antigens (Fig. 2e), where MEF2B protein expression appeared in activated B cells soon after immunization (day 2), slightly preceded that of Bcl-6, a known marker of GC commitment, and was co-expressed with Bcl-6 throughout the GC reaction, as confirmed by immunofluorescence staining (Fig. 2e and Supplementary Fig. 2a,b). These observations indicate that MEF2B, similarly to Bcl-6, is a *bona fide* GC B cell marker.

MEF2B directly regulates *BCL6* transcription

The coexpression of MEF2B and Bcl-6 in GC B cells prompted us to investigate the relationship between these two transcription factors. Analysis of the Human B cell Interactome (HBCI)[28], showed that MEF2B was specifically connected to Bcl-6 and ZMYND11, which showed positive (red line, Bcl-6) and negative (green line, ZMYND11) transcriptional relationships with MEF2B, as shown in the Circos plot[29] (Fig. 3a). Accordingly, *MEF2B* gene expression displayed a strong positive correlation with *BCL6* in a variety of B cell phenotypes (Fig. 3b), and appears to be a main node in the Bcl-6 regulatory network predicted by the ARACNe algorithm[30], a reverse engineering approach applied on a large dataset of normal and malignant B cells.

While the *MEF2B* gene was not included among the list of direct transcriptional targets bound by Bcl-6 *in vivo*[31], we identified several AT-rich DNA sequences resembling canonical MEF2 binding motifs in a ∼1.5 kb *BCL6* promoter region proximal to the transcription start site (TSS) (Supplementary Fig. 2c), suggesting that MEF2B could bind the *BCL6* promoter region. In support of this hypothesis, chromatin immunoprecipitation (ChIP) in tonsillar GC B cells and in two DLBCL cell lines (U2932, SUDHL4) revealed binding of MEF2B to a region on the *BCL6* promoter located approximately 1 kb upstream of the *BCL6* TSS (Fig. 3c and Supplementary Fig. 2c,d). To determine the transcriptional outcome of MEF2B binding to the *BCL6* promoter, we analyzed the response to MEF2B of a luciferase reporter gene driven by a native *BCL6* promoter region (−1593 to −672). Co-transfection of this reporter with increasing amounts of a wild-type MEF2B expressing

plasmid (HA-MEF2B) in HEK293T cells led to a dose-dependent increase in the reporter activity (up to five-fold) (Fig. 3d). While both MEF2B isoforms were able to transactivate the *BCL6* reporter construct, isoform B (Fig. 3d) exhibited higher transcriptional activity than isoform A, both in HEK293T and in DLBCL cells (Supplementary Fig. 3). Deletion of the DNA binding and dimerization domains of MEF2B (HA-MEF2BΔMADSMEF2), or selective mutation of a potential MEF2B consensus site in the *BCL6* promoter region, abrogated the ability of MEF2B to transactivate the *BCL6* promoter, thus confirming the specificity of the observed transcriptional effects (Fig. 3d and Supplementary Fig. 3).

To demonstrate the relevance of the MEF2B-dependent regulation of Bcl-6 expression *in vivo*, we silenced MEF2B in two DLBCL cell lines: U2932 and SUDHL4, using two different short hairpin RNAs that can target both isoforms of MEF2B. Consistent with the luciferase reporter assays, knockdown of MEF2B led to down-regulation of Bcl-6 expression, while knockdown of Bcl-6 did not affect MEF2B protein or mRNA expression (Fig. 3e and Supplementary Fig. 4). Accordingly, silencing of MEF2B expression in DLBCL cell lines (LY8 and VAL) carrying *BCL6* translocations that remove the MEF2B-bound region on the *BCL6* promoter did not affect Bcl-6 protein expression (Fig. 3f), in contrast to what could be observed in DLBCL cell lines with wild-type *BCL6* alleles (U2932 and SUDHL4; Fig. 3e). Finally, MEF2B knockdown in a B cell line (P3HR1) led to increased expression of Bcl-6 target genes[31] (Supplementary Fig. 4). Taken together, these data demonstrate that *BCL6* is a direct transcriptional target of MEF2B in normal and malignant GC B cells.

MEF2B is required for DLBCL proliferation

To investigate whether, like Bcl-6, MEF2B is required for DLBCL growth, we infected the SUDHL4 (D83V *MEF2B* mutation) and the U2932 (wild-type *MEF2B*) cell lines with an inducible lentiviral vector system in which transcription of a turboRFP (tRFP)-shRNA cassette is dependent upon the addition of doxycycline (Dox)[32] (Fig. 4a). In SUDHL4 cells, two different MEF2B shRNAs caused a progressive depletion of targeted cells (tRFP+), in direct correlation with their ability to decrease MEF2B mRNA and protein abundance (Fig. 4a,b and Supplementary Fig. 4). This growth defect was associated to a substantial decrease in Bcl-6 mRNA and protein expression, and it was not observed when using a control shRNA (Fig. 4a,b and Supplementary Fig. 4). As expected, knockdown of Bcl-6 resulted in defective cell growth, with no effect on MEF2B expression (Fig. 4a,b). Cell cycle distribution analysis by flow cytometry revealed that tRFP+ SUDHL4 cells expressing either MEF2B or Bcl-6 shRNAs were mainly arrested at the G1 phase of the cell cycle (Fig. 4c and Supplementary Fig. 4), while no increase was observed in early apoptosis (Annexin V) or cell death (7-AAD) markers (data not shown). Similar results were obtained for the U2932 cells (data not shown). Enforced expression of Bcl-6 alone was not sufficient to rescue the proliferative defects of B cells upon MEF2B knockdown, (Supplementary Fig. 5). Therefore, GC-derived lymphoma cells are dependent on MEF2B for their growth and proliferation, and this effect is only in part related to its ability to control Bcl-6 expression.

N-terminal mutations enhance MEF2B transcriptional activity

We then investigated the consequences of DLBCL- and FL-associated *MEF2B* mutations on the MEF2B-Bcl-6 axis by examining all *MEF2B* mutations that were detected in our panel (Supplementary Table 1), as well as two additional somatic missense mutations (Y69H and N81Y), which are highly recurrent in DLBCL and FL[5]. Analysis of the transcriptional response to these different mutants on a luciferase reporter construct driven by the *BCL6* promoter region showed that a subset of mutations located in the N-terminal half of MEF2B, including the most recurrent D83V, displayed increased transcriptional activity (Fig. 5a and Supplementary Fig. 3). The enhanced transcriptional activity of these mutations suggested a probable dominant effect, as all these *MEF2B* mutations are found in heterozygosity in primary DLBCL cases. This notion was confirmed by showing that co-transfection of equimolar amounts of wild-type MEF2B and MEF2B D83V mutant, mimicking the situation observed in primary DLBCL, caused an increase in *BCL6* promoter transactivation similar to the D83V alone (Supplementary Fig. 6).

To confirm the physiologic relevance of these findings, we investigated the Bcl-6 transcriptional signature[31], as a proxy of Bcl-6 activity, in the gene expression profiles of primary DLBCL cases stratified by the presence or absence of *MEF2B* mutations. Using the GSEA tool[33], we observed that DLBCL cases carrying mutant *MEF2B* alleles with enhanced transcriptional activity showed significant downregulation of Bcl-6 target genes[31] (NES=2.05, *P*-value < 0.00001) (Fig. 5b). This result suggested that MEF2B mutants, displaying enhanced transcriptional activity on the *BCL6* promoter, lead to increased Bcl-6 biological activity and, thus, may contribute to the deregulation of this proto-oncogene in DLBCL and FL.

N-terminus mutants escape CABIN1 co-repressor activity

To identify the mechanisms by which lymphoma-associated MEF2B mutants affect its transcriptional activity, we used publicly available structural data of the human N-terminus MEF2B domain complexed with DNA and with its known co-repressor, CABIN1[20] (Fig. 6a). Using the PyMol software (http://www.pymol.org/) to study potential structural alterations due to mutated residues, we predicted that several *MEF2B* missense mutations (L54P, Y69H, E77K, S78R and D83V) could impair the ability of MEF2B to bind the CABIN1 co-repressor (Fig. 6a and Supplementary Table 1). Additionally, the L38I, L54P and N81Y mutations may alter the homodimerization of MEF2B, while K4E may affect DNA binding (Fig. 6a and Supplementary Table 1).

To test these predictions, we performed co-immunoprecipitation assays to investigate the ability of wild-type and MEF2B mutants to interact with CABIN1 upon co-transfection in HEK293T cells. Six mutations (L54P, Y69H, E77K, S78R, N81Y and D83V) abrogated binding of MEF2B to CABIN1, while the remaining mutants behaved similarly to wild-type MEF2B (Fig. 6b). With the only exception of N81Y, all these mutations displayed increased transcriptional activity on *BCL6* (Fig. 5a). The physiologic nature of the interaction between wild-type MEF2B and CABIN1 was confirmed for endogenous proteins in normal GC B cells and in U2932 and SUDHL10 DLBCL cells (Fig. 6c and Supplementary Fig. 7). However, this physiologic interaction was partially abrogated as a consequence of the D83V

heterozygous mutation present in SUDHL4 and DB DLBCL cells, which express only residual amounts of the remaining wild-type protein (Fig. 6c and Supplementary Fig. 7). No interaction between native wild-type MEF2B and HDAC9, a class II HDAC reported to interact with MEF2B and other MEF2 family members, was observed in GC B cells or DLBCL cell lines (Fig. 6c and Supplementary Fig. 7). In agreement with these observations, ChIP assays in a wild-type MEF2B DLBCL cell line (U2932) confirmed the presence of endogenous CABIN1 at the *BCL6* promoter in the MEF2B-bound region (Fig. 6d). In contrast, MEF2B failed to recruit CABIN1 to the *BCL6* promoter in SUDHL4 DLBCL cells (Fig. 6d), which carry a *MEF2B* mutation (D83V) that abrogates binding to CABIN1 (Fig. 6b,c) and furthermore display higher Bcl-6 protein levels when compared to other DLBCL cell lines with similar MEF2B expression (Supplementary Fig. 7b).

Accordingly, the L54P, Y69H, E77K, S78R, N81Y and D83V mutant proteins that failed to bind CABIN1 in co-immunoprecipitation assays (Fig. 6b,c) and to recruit CABIN1 to the *BCL6* promoter (Fig. 6d), also escaped the co-repression effects of CABIN1 in promoter reporter assays (Fig. 6e). Reciprocally, an experimentally generated L2172A mutation in CABIN1, which abrogates binding to MEF2B[20], blocked this co-repressive effect, thus confirming the specificity of the MEF2B-CABIN1 interaction (Supplementary Fig. 7). Analogous results were obtained when the same mutations were assayed in the context of MEF2B isoform A (Supplementary Fig. 3). An exception to the above observations was the L38I mutant, which did not respond to CABIN1 despite its ability to physically interact with this transcriptional co-repressor (Fig. 6b,e; see Supplementary Fig. 8 legend for details). Although L38I and two other missense mutations (L54P and N81Y) were suggested to affect the dimerization of MEF2B monomers based on the crystal structure (Fig. 6a), we did not observe altered homodimerization in co-immunoprecipitation assays (Supplementary Fig. 8a), suggesting that these three mutations may instead stabilize the MEF2B dimer (Supplementary Fig. 8 legend).

Overall, these results indicate that a subset of lymphoma-associated MEF2B mutations abrogate binding to CABIN1 and response to its co-repressive activity, resulting in deregulated MEF2B transcriptional activity. Considering both the confirmation from biochemical analyses and the structural predictions, this mechanism accounts for 56% of all DLBCL- and FL-cases with *MEF2B* mutations reported thus far (n = 47/90 and n = 3/90, respectively)[4–6].

C-terminal mutations impair negative regulation by PKA

The predominance of nonsense and frameshift mutations leading to truncated MEF2B proteins suggested that these mutations may have been selected for the elimination of a C-terminal regulatory domain (Fig. 1a). This observation, together with the finding that protein kinase A (PKA) phosphorylates the C-terminus of MEF2D and abrogates its transactivation activity[34], prompted us to explore whether MEF2B is similarly regulated by PKA, a serine/threonine protein kinase whose activity is dependent on cytoplasmic concentrations of cyclic AMP (cAMP)[35].

To investigate whether MEF2B is phosphorylated by PKA *in vivo*, we performed MEF2B immunoprecipitation upon ^{32}P metabolic labeling of SUDHL4 DLBCL cells in the presence

of Forskolin (FSK), an activator of adenylate cyclase[36] and PKA (Fig. 7a). The basal phosphorylation content of endogenous MEF2B was substantially enhanced upon FSK addition and completely blocked in the presence of H89, an established PKA small molecule inhibitor[37], indicating the specific involvement of this kinase (Fig. 7a). We also observed additional phosphorylated high molecular weight bands in the immunoprecipitates, which could correlate with other covalent modifications of MEF2B (e.g. sumoylation, see below). In contrast, both the R171X and Y201X mutants, which encode the largest truncated MEF2B proteins, were not phosphorylated in response to FSK (Fig. 7b), thus suggesting that MEF2B, and more specifically its C-terminus, is indeed targeted by PKA-dependent phosphorylation.

To test the functional consequence of PKA phosphorylation, we examined its effect on the ability of MEF2B to regulate *BCL6* transcription in transient luciferase reporter assays. Similar to previous reports on MEF2D negative regulation by PKA[34], MEF2B transcriptional activity was substantially decreased in the presence of FSK treatment (Fig. 7c) or exogenous PKA (Fig. 7d), but not in the presence of a PKA kinase-dead mutant (K72H)[38]. Notably, both the R171X and Y201X mutants escaped the negative regulation by PKA (Fig. 7c,d), consistent with the absence of FSK-induced phosphorylation on these mutants (Fig. 7b). Thus, DLBCL-associated MEF2B C-terminal truncations disrupt the negative regulatory effects of PKA-dependent phosphorylation.

Frameshift and nonsense mutations abrogate MEF2B sumoylation

In considering the effect of the three frameshift mutations (G242fs, P256fs, and L269fs) affecting the most C-terminal portion of the MEF2B protein, we noted that they are predicted to cause the switch from isoform A to isoform B (Supplementary Fig. 1). The latter isoform lacks a highly conserved phosphorylation-dependent sumoylation motif (PDSM)[39] found in all MEF2 family members (Fig. 8a). This domain would also be lost in all alleles carrying premature truncating mutations. The PDSM is a bipartite motif composed of a SUMO consensus site (ψKxE) and a proline-directed phosphorylation site, separated by two amino acids (ψKxExxSP) (Fig. 8a). The negative charge conferred by phosphorylation of the serine residue within the PDSM facilitates sumoylation of the lysine residue through recruitment of the E2 conjugating enzyme, Ubc9[40].

To determine whether MEF2B isoform A is sumoylated at the putative K319 sumoylation site within the MEF2B PDSM, we assessed whether MEF2B could be modified *in vivo* in the presence of SUMO1 and the E2 conjugating enzyme Ubc9, in transient transfection assays. Wild-type isoform A, but not isoform B, of MEF2B was specifically sumoylated at K319, since mutation of this residue to an arginine greatly impaired sumoylation (Fig. 8b). The shift in the molecular mass of MEF2B by ∼15 kDa, suggests that MEF2B was modified by monosumoylation at this site (Fig. 8b). Notably, the serine residue within the PDSM of MEF2B isoform A (green box, Fig. 8a) appears to be embedded within a potential PKA consensus site (RxS/T). Mutation of this serine residue (S324) to alanine greatly impaired both FSK-dependent phosphorylation of MEF2B (Fig. 8c) and sumoylation of MEF2B (Fig. 8b), suggesting that MEF2B sumoylation is dependent on PKA-mediated phosphorylation at this site within the PDSM consensus. Notably, both the C-terminal truncated R171X and

Y201X MEF2B mutants were not sumoylated in the same assay (Fig. 8b), consistent with the loss of the sumoylation site at residue 319. Predictably, this highly conserved sumoylation motif is also lost in all frameshift mutations switching from isoform A to B, as the latter lacks the PDSM consensus.

We then tested whether this post-translational modification modulated MEF2B transcriptional activity as it is the case for other MEF2 proteins[41,42]. Indeed, sumoylation of MEF2B in the presence of SUMO1 and Ubc9 substantially reduced wild-type MEF2B transcriptional activity (Fig. 8d), whereas mutations of both K319 and S324 in the PDSM consensus significantly impaired this negative effect on MEF2B activity (Fig. 8d, wild-type vs K319R-S324A). The presence of SUMO1-Ubc9 failed to reduce the transcriptional activities of the DLBCL-associated MEF2B mutants, R171X and Y201X (Fig. 8d), consistent with the loss of the PDSM consensus in these alleles and the absence of sumoylation on these mutants *in vivo* (Fig. 8b).

Together, these results show that phosphorylation-dependent sumoylation negatively regulates the transcriptional activity of MEF2B in B cells. Thus, the vast majority of lymphoma-associated mutant alleles affecting the C-terminus of MEF2B (73%, 11/15), escape from this negative regulation. Overall, PKA- and sumoylation-mediated regulation of MEF2B is predicted to be lost in ∼12% (11/90) of all reported *MEF2B*-mutated cases[4–6].

DISCUSSION

Our results suggest that MEF2B may actually be a hierarchically relevant transcription factor responsible for the initiation of a broad program of gene expression that substantially defines the GC B cell phenotype. Part of this broad MEF2B transcriptional program appears to rely on its ability to modulate Bcl-6 expression, a key factor in GC biology that modulates cell cycle, plasma cell differentiation, the responses to DNA damage, and anti-apoptotic molecules such as BCL2[26]. While our results suggest an apical role of MEF2B in instructing the GC phenotype, and indicate that Bcl-6 may represent one mediator of its function, additional analyses are necessary to comprehensively define the role of this transcription factor in GC formation.

The critical role of MEF2B in the regulation of GC formation is consistent with its targeting by genetic alterations in DLBCL and FL, which represent malignant phenotypes of the GC. Overall, ∼11% of DLBCL and 12% of FL cases[4–6] tested so far carry mutations of the *MEF2B* gene. Our results indicate that *MEF2B* mutations have important functional consequences through at least three distinct mechanisms, which differ by the nature and position of the mutations, leading to deregulated MEF2B activity.

The first and most frequent set of mutations affect the N-terminal domain of the protein and represent gain-of-function mutations that enhance the transcriptional activity of MEF2B by preventing its binding to the CABIN1 co-repressor and by blocking CABIN1 co-recruitment to the MEF2B-bound genomic regions. Notably, another MEF2 family member, MEF2C, is also targeted by mutations in ∼2% of DLBCL cases[5,6], which affect exclusively the conserved N-terminal MADS-box/MEF2 domain known to recruit transcriptional

coactivators and corepressors. In fact, residue Y69, which is involved in the binding to CABIN1, is also mutated in MEF2C, suggesting a common theme in the selection of MEF2 family member mutations during B cell lymphomagenesis. However, different from what has been described for the other MEF2 family members, we could not detect physical interaction between MEF2B with the co-activator EP300 or its related acetyltransferase molecule CREBBP in co-immunoprecipitation assays (data not shown). Finally, an additional ∼26% (23/90) of mutant cases, which carry MEF2B variants in the N-terminus, probably do not involve the above mechanism. For these mutants, alternative mechanisms can be invoked based on structural predictions and previous reports, i.e. the altered affinity for DNA (predicted for G2E, K4E, K5E, I8V, R15G, K23V mutations) or for basic helix-loop-helix (bHLH) protein partners[43].

A second less frequent set of cases contain mutations that affect the C-terminus of the protein, and encode MEF2B proteins still capable of CABIN1 binding, but carrying a distinct C-terminus due to either truncating nonsense/frameshift mutations or, more rarely, to frameshift mutations causing the switch from isoform A to a predominant production of isoform B proteins. These mutations cause the escape of MEF2B from PKA-mediated phosphorylation and sumoylation, which probable render MEF2B insensitive to upstream signals of yet unclear nature. We note that PKA-mediated phosphorylation of MEF2B may be relevant, given the importance of PKA activity in GC physiology, where it is required for the activation of AICDA[44,45] and thus for somatic hypermutation of immunoglobulin genes and antibody affinity maturation. Therefore, by a different mechanism, i.e. resistance to negative regulatory modifications, the second group of MEF2B mutants (C-terminus) may also cause deregulated transcriptional activity of MEF2B.

While transcriptional deregulation of *BCL6* is unlikely to be the only consequence of MEF2B aberrant activity, it is clearly a relevant contributor to lymphomagenesis, as shown by the presence of chromosomal translocations deregulating *BCL6* expression in DLBCL and FL[46,47], and by the demonstration that these events contribute to lymphomagenesis in transgenic mice[48]. Mutational deregulation of MEF2B may represent an additional mechanism leading to *BCL6* deregulation in alternative to those previously described, including aberrant transcriptional regulation by promoter substitution caused by chromosomal translocations[49], mutations in the *BCL6* promoter sequence[16], defective acetylation in cases displaying inactivating mutations of CREBBP or EP300[8], or defective ubiquitin/proteasome-mediated degradation due to inactivating mutations of the ubiquitin ligase FBXO11[50]. In agreement with this observation, *BCL6* chromosomal rearrangements appear to be mutually exclusive in DLBCL cases carrying *MEF2B* activating mutations[5], supporting the idea that both types of lesions are acting in the same oncogenic pathway.

In conclusion, the clear functional significance of the large fraction of *MEF2B* mutations characterized so far, strongly suggests their selection for a role in lymphomagenesis. Their distribution in both GCB- and ABC-type DLBCL, as well as in FL suggests a general role in transformation common to all subtypes. Finally, given the dependency of DLBCL cells on MEF2B for their normal growth, and the current efforts on the pharmacological inactivation of Bcl-6[51] as a targeted strategy for the treatment of these malignancies, the results herein

suggest that MEF2B may represent a therapeutic target for the inhibition of Bcl-6 activity and possibly of a broader GC program to which mature B cell lymphomas may be addicted.

METHODS

Primary samples and mutation analysis

High molecular weight genomic DNAs from 111 newly diagnosed DLBCL samples and 35 FL cases were studied under protocols approved by the Institutional Review Board of Columbia University. This research involved coded information on archival biological specimen and is classified as Exempt Human Subject Research of anonymized/de-identified existing pathological specimens, under regulatory guideline 45 CFR 46.101(b)(4). The fraction of tumor cells, assessed by Southern blot analysis of the rearranged immunoglobulin heavy chain locus and/or by histological analysis of frozen sections isolated before and after obtaining tissue for molecular studies, corresponded to >80% in most cases and to >50% in all cases. Detailed characterization of the DLBCL cohort (cell lines and primary biopsies) including classification by gene expression profile analysis into the ABC or GCB subtypes have been previously reported[4,13].

The *MEF2B* coding exons were subjected to targeted DNA sequencing by the Sanger method on PCR products obtained from whole genome amplified DNA using the oligonucleotides reported in Supplementary Table 2. Mutations were confirmed by PCR amplification and double-strand DNA sequencing of independent products obtained from genomic DNA. Somatic origin was verified by analysis of paired normal DNA, where available.

All mutations reported[4–6] were verified for their absence in reported SNP databases. Mutations R114Q and R307Q from Morin *et al*., 2011 (ref. 5) are reported in dbSNP build 135 and were thus excluded.

Cell lines

HEK293T cells (ATCC) were grown in Dulbecco's Modified Eagle Medium (DMEM) supplemented with 10% fetal calf serum, 100 μg/ml penicillin and streptomycin. The DLBCL cell lines SUDHL4, U2932, SUDHL10, DB, LY8, VAL and BJAB were grown in Iscove's Modified Dulbecco Medium (IMDM) supplemented with 10% fetal calf serum, 100 μg/ml penicillin and streptomycin. All cell lines were tested negative for mycoplasma contamination.

Chromatin immunoprecipitation (ChIP)

ChIP assays were performed using purified $CD77^+$ GC B cells[25] or DLBCL cell lines (SUDHL4 and U2932) as previously described[16]. Briefly, crosslinked chromatin was fragmented by sonication with the Bioruptor (Diagenode) or alternatively with Covaris S220 to reach a ∼300–500 bp size. MEF2B antiserum (ab3350, Abcam), CABIN1 antiserum (ab3349, Abcam), or isotype-matched polyclonal IgG (Sigma-Aldrich) were used for chromatin immunoprecipitation. Quantitative PCR reactions on ChIP DNA (qChIP) were performed using the ABsolute QPCR SYBR green mix (Thermo Scientific) in a 7300 Real

Time PCR system (Applied Biosystems). Primers spanning the ∼1.5 kb proximal promoter region of *BCL6* (see Supplementary Table 2) were used to define the peak of MEF2B binding in that region (as shown in Supplementary Fig. 2c). Primer pair selection was limited by the efficiency of target site/region amplification. For the qChIP analysis shown in Fig. 3c, Fig. 6d, the primer pair used were 'B6prom_Tiling_F5' and 'B6prom_Tiling_R5', which correspond to the main peak of MEF2B binding in the *BCL6* promoter (−1167/−971 relative to the TSS). ΔCt values were calculated for anti-MEF2B, anti-CABIN1 and control IgG immunoprecipitated DNA fragments relative to the input DNA. Fold enrichments observed in MEF2B or CABIN1 immunoprecipitates versus IgG immunoprecipitated DNA were further normalized to the enrichments observed for the *ACTB* gene locus, used as negative control locus, and reported as relative fold enrichment in the graphs. Of note, we observed substantial variations in immunoprecipitation efficiencies between batches of MEF2B-specific antibody (ab3350; Abcam).

Expression constructs, transient transfections and luciferase reporter assays

MEF2B and CABIN1 (residues 2037–2220) were amplified by PCR from human normal GC B-cell cDNA. GenBank accession numbers for the reference sequence are NM_001145785.1 (MEF2B isoform A), NM_005919 (MEF2B isoform B) and NM_001199281.1 (CABIN1). These cDNAs were subcloned into pCMV vectors with an HA-, Myc- (Clontech), or Flag-tag (Stratagene) for expression in mammalian cells. MEF2B missense and nonsense mutant expression constructs were generated by site-directed mutagenesis using the mammalian expression vector encoding the wild-type human MEF2B as a template. The 31 bp deletion (L269fs) was obtained by PCR amplification using the pCMV-MEF2B isoform A expression vector as a template; the final L269fs mutant construct was completed by ligating to the C-terminal fragment (NaeI and NotI sites) of isoform B. The MADS-box/MEF2 domain deletion (deleted residues 8–91) was generated by PCR amplification using pCMV-MEF2B as a template. The CABIN1 coding sequence (residues 2037–2220) was amplified by PCR using cDNA from human GC B-cells and subcloned into pCMV-Myc tag expression vector (Clontech). CABIN1_L2172A mutant was generated by site-directed mutagenesis using the mammalian expression vector encoding for the wild-type CABIN1 (residues 2037–2220) as a template. pCMV-HA tagged PKACA was previously generated[44], and was used as a template to generate a kinase-dead PKA mutant (K72H) by site-directed mutagenesis. pcDNA3-Ubc9 (Addgene plasmid 20082) was purchased from Addgene (deposited by E. Yeh). HA-tagged SUMO1 was a generous gift from R.T. Hay. Luciferase reporter construct (*BCL6*-luc) was generated by cloning a 921 bp HindIII-HindIII (−1593 to −672) fragment of the *BCL6* promoter digested from the previously generated pLA/S5wt construct[16] into pGL4.26 and pNL1.1 vectors (Promega). All final constructs were verified by digestion and confirmed by Sanger sequencing analysis.

Transient transfections in HEK293T cells were performed using polyethylenimine (PEI, Polysciences) as described[52]. Transient transfections in BJAB cells were performed using Lipofectamine LTX (Invitrogen) according to the manufacturer's instructions.

Equimolar amounts of wild-type and mutant pCMV-MEF2B vectors were cotransfected with the *BCL6*-luc reporter construct (pGL4.26 vector) and the Renilla luciferase control

reporter (pRL-SV40) in the presence or absence of the pCMV-myc-CABIN1 expression vector. Cells were harvested 48 h after transfection, and the Dual Luciferase Reporter Assay (Promega) was performed according to the manufacturer's instructions. Cells transfected with the *BCL6*-luc reporter construct (pNL1.1 vector) were harvested and processed for the Nano-Glo Luciferase Assay (Promega) according to the manufacturer's instructions.

Lentiviral transductions

Lentiviral vectors (pLKO.1) expressing MEF2B shRNA#1 (TRCN0000232095; 5′-*CCGGGGACTAAACACCTCCAGAAGCCTCGAGGCTTCTGGAGGTGTTTAGTCCTTTTTG*-3′); MEF2B shRNA#2 (TRCN0000015738; 5′-*CCGGCGGCGACTTTCCTAAGACCTTCTCGAGAAGGTCTTAGGAAAGTCGCCGTTTTT*-3′); Bcl-6 shRNA#1 (TRCN0000013603; 5′-*CCGGCCCATGATGTAGTGCCTCTTTCTCGAGAAAGAGGCACTACATCATGGGTTTTT*-3′); Bcl-6 shRNA#2 (TRCN0000013606; 5′-*CCGGCCACAGTGACAAACCCTACAACTCGAGTTGTAGGGTTTGTCACTGTGGTTTTT*-3′); and a control shRNA (SHC002) were purchased from Sigma. Viral supernatants were obtained by transiently transfecting HEK293T cells with the lentiviral vectors along with Δ8.9 and VSVg encoding vectors, and were used to infect SUDHL4 and U2932 as previously described[13]. These shRNAs correspond to experiments in Fig. 3.

The mir30-based hairpins: MEF2B (a) shRNA (V2LHS 253202; pGIPZ vector; mature anti-sense sequence, 5′-*ACTCTGTGTACTTCAGCAG*-3′) was purchased from Open Biosystems and subcloned into the pINDUCER11 inducible lentiviral vector[32]. MEF2B (b) shRNA (5′-*TGCTGTTGACAGTGAGCGATCCGGTCAGCATCAAGTCTGATAGTGAAGCCACAGATG TATCAGACTTGATGCTGACCGGAGTGCCTACTGCCTCGGA*-3′); Bcl-6 (a) shRNA (5′-*TGCTGTTGACAGTGAGCGAAAGGTGCAATACCGCGTGTCATAGTGAAGCCACAGATG TATGACACGCGGTATTGCACCTTGTGCCTACTGCCTCGGA*-3′); and Bcl-6 (b) shRNA (5′-*TGCTGTTGACAGTGAGCGCACTGGAAGAAATACAAGTTCATAGTGAAGCCACAGATGT ATGAACTTGTATTTCTTCCAGTTTGCCTACTGCCTCGGA*-3′) were designed following the 'sensor' rules[53], and cloned into the pINDUCER11 lentiviral vector[32]. 2×10^6 SUDHL4 and U2932 cells were infected with two rounds of viral supernatants (MEF2B shRNAs, Bcl-6 shRNAs or control shRNA targeting the Renilla luciferase gene[54]). Cells were treated with doxycycline (DOX, 1 μg/ml) for induction of the tRFP-shRNA cassette. To obtain $tRFP^+$ and $tRFP^-$ pure populations for mRNA and protein analysis, exponentially growing cultures of infected cells were sorted using a FACSAria II flow cytometer/sorter (HICCC Flow Cytometry Facility). Cells with $>10^2$ tRFP MFI were collected, pelleted and lysed for analysis. These shRNAs were used in the experiments shown in Fig. 4.

Co-immunoprecipitation assays

In transient assays and 48 h after transfection, HEK293T cells were lysed in IP buffer: 50 mM Tris, pH 7.05, 250 mM NaCl, 1 mM EDTA, 1% Triton X-100, 0.05% NP40, 1 mM NaF, 10 mM beta-glycerophosphate, 0.5 mM PMSF, protease inhibitors. Lysates were incubated overnight with anti-HA affinity beads (Sigma) at 4 °C. Beads were washed in the

same buffer, and bound proteins were eluted in the presence of 0.25 mg/ml HA peptide (Sigma). Eluates were resolved by SDS-PAGE and analyzed by immunoblot.

Nuclear extracts were generated from SUDHL4 and U2932 cells as previously described[55]. Lysates were incubated overnight with the MEF2B antibody (Abcam) at 4°C, and supplemented with Protein G beads (GE Healthcare) for 1 h at 4°C. Beads were washed 5 times in Wash Buffer (20 mM HEPES, pH 7.9, 300 mM NaCl, 1.5 mM $MgCl_2$, 1 mM EDTA, 0.2% NP40, 10 mM beta-glycerophosphate, 0.5 mM PMSF, protease inhibitors); immunocomplexes were eluted in SDS-PAGE sample loading buffer, and the eluates were resolved by SDS-PAGE for immunoblot analysis.

To allow detection of *in vivo* sumoylation events (HA-tagged SUMO1), 25 mM N-ethylmaleimide (NEM, Sigma) was added during lysis and was maintained throughout the IP procedure.

In vivo metabolic labeling with ^{32}P-orthophosphate

To radioactively label the phosphorylated form of endogenous MEF2B in SUDHL4 cells, cell cultures were pre-incubated for 1 h in DMEM without phosphates and with 10% dialyzed FCS (Gibco/Life Technologies). ^{32}P-orthophosphate (67 μCi/ml) was subsequently added and cells were grown at 37 °C for 6 h in presence of 10 mM HEPES, pH 7.0 (Gibco/Life Technologies) in a shielded incubator, with or without addition of 20 μM Forskolin (Sigma) and/or 40 μM H89 (Cell Signaling). Cells were then washed in cold PBS, lysed in IP buffer supplemented with phosphatase inhibitors (sodium orthovanadate and sodium fluoride), and endogenous MEF2B was immunoprecipitated with anti-MEF2B (Abcam). Immunoprecipitates were resolved by SDS-PAGE, and the gel was dried and exposed to autoradiography films overnight at −80 °C. A fraction of the immunoprecipitates was transferred to nitrocellulose membranes for immunoblot analysis.

Cell cycle analysis

For cell cycle analyses, cells were labeled by the addition of 10 mM BrdU to the culture media for 2 h before harvesting. BrdU (active DNA synthesis) and 7-AAD (DNA content) were detected using the APC BrdU detection kit (BD Biosciences), as per manufacturer's instructions. Stained cells were analyzed using a FACSCalibur flow cytometer (BD Biosciences), gating on tRFP positive high subpopulations. Final data analysis and plot rendering were done using FlowJo 9.5.2 software (TriStar).

Structural analysis

PyMOL software (http://www.pymol.org/) was used to map and assess the molecular interactions of DLBCL-associated MEF2B mutations onto the crystal structures of MEF2B/CABIN1 and MEF2A/EP300. The coordinates used to generate the structural view were retrieved from the RCSB Protein Data Bank under accession codes 1N6J (CABIN1/MEF2B/DNA ternary complex) and 3P57 (EP300/MEF2A/DNA ternary complex).

RNA extraction, cDNA synthesis and quantitative real-time PCR

Total RNA was extracted from DLBCL cell lines, naive B cells and GC B cells by Trizol reagent (Invitrogen) according to the manufacturer's instructions. cDNA was synthesized using the SuperScript II™ First-Strand Synthesis System (Invitrogen). For detection of the normal and mutant *MEF2B* alleles in the primary DLBCL cases, primers surrounding the mutation site were designed (Supplementary Table 2) and the amplified PCR products were analyzed by direct sequencing. qRT-PCR was performed using the primers shown in Supplementary Table 2 and the ABsolute QPCR SYBR green mix (Thermo Scientific) in the 7300 Real Time PCR system (Applied Biosystems). GAPDH was used as negative control for qRT-PCR. QPCR reactions were performed in triplicates.

Immunoblotting

Immunoblot analysis was performed by incubating the membranes after 1 h of blocking in PBS-0.2%Tween-5% milk in dilutions of the primary antibodies in PBS-0.2%Tween-3% BSA overnight at 4 °C (except for anti-ACTB, 21 °C for 1 h) with constant rotation. The commercial antibodies used are detailed in Supplementary Table 3. Densitometry was performed using ImageJ software (Fig. 6 and Supplementary Fig. 7).

Immunofluorescence analysis on paraffin-embedded lymphoid tissues

Immunofluorescence analysis was performed on 3 μm-thick sections of formalin-fixed, paraffin- embedded tissues, as previously described[56]. Briefly, heat-induced epitope retrieval was performed in citrate buffer (pH 6.0). All primary antibody incubations were performed at 4 °C overnight. After repeated washes in PBS-0.1%Tween, tissue sections were incubated with fluorochrome-, HRP- or biotin-conjugated species and isotype-specific secondary antibodies (1 h, 21 °C, washed and mounted (ProLong Gold Anti-Fade Reagent, Invitrogen). To avoid cross-reactions when using mouse Bcl-6 specific antibodies on mouse tissues, an anti-mouse IgG1 specific secondary was used, which yields minimal background in mouse germinal centers. For MEF2B immunodetection in human and mouse tissues, a polymer-enhanced HRP-conjugated secondary antibody (EnVision+ system, Dako) was used, and immunocomplexes were detected using Tyramide-fluorochrome amplification (Perkin-Elmer; 1:1000 for 3 min). For biotin-conjugated primary and secondary antibodies (PAX5 immunodetection on human tissues, and B220 immunodetection in mouse tissues), streptavidin-fluorochrome was added as a final step. Antibody details are provided in Supplementary Table 3.

Mouse immunization and tissue collection

C57BL/6 mice were purchased from The Jackson Laboratory and housed in a dedicated pathogen–free environment. All experiments and procedures were conformed to ethical principles and guidelines, revised and approved by the Institutional Animal Care and Use Committee at Columbia University.

4-month-old mice were immunized with a single intraperitoneal injection of sheep red blood cells (SRBC) to trigger T cell-dependent immune responses, and sacrificed at different times from immunization (2,3,4,5 days; 2 mice per time point). Spleens were then isolated and

divided in two fragments, which were processed for histologic and flow cytometry analyses, as previously described[56]. Splenic mononuclear cells were isolated by straining the tissue through 40 micron meshworks in PBS-0.5%BSA buffer, and lysing the red blood cells as reported[56]. Mononuclear cell suspensions were stained with antigen-specific fluorochrome-conjugated antibodies for 20 minutes on ice (antibodies are detailed in Supplementary Table 3), and analyzed using a BD LSR II Flow cytometer (BD Biosciences). 200,000 events were collected per sample and analyzed using the FlowJo Software (TriStar, V. 9.5.2).

Bioinformatic Analyses

To generate the Human B-Cell Interactome (HBCI), we first generated a transcriptional network from a large compendium of 199 B-cell gene expression profiles, using Affymetrix HG-U95Av2 GeneChip, representing normal B cell types isolated from human tonsils and B cell tumors[30]. The transcriptional network was generated using the bootstrap version of the ARACNe algorithm[57] with parameters: *P*-value = 1e–7, dpi = 0 and 100 bootstraps. To generate the final HBCI, we used the Bayesian evidence integration algorithm to integrate transcriptional network with evidences from experimental assays, databases and literature mining, by filtering them in a context-specific criteria, as explained in previous publications[28]. The HBCI contains about 38,500 B-cell specific interactions including both protein-protein and protein-DNA interactions.

To discover Master Regulators (MRs) of GC, we interrogated the HBCI using the MAster Regulator INference Algorithm (MARINa)[28]. Briefly, this algorithm first identifies the positive and negative regulon of each transcription factor (TF) by computing the Spearman correlation between the expression profile of the TF with each of its targets from HBCI. Second, it computes the enrichment of the regulon of each TF on the genes differentially expressed between GC B-cells (10 samples) vs. naive B-cells (5 samples) using GSEA[33]. We computed the enrichment for 308 TFs with at least 20 targets and ranked all TFs based on the Differentially Expressed Target Odds Ratio (DETOR), which is defined as the ratio of the % of genes from the regulon before the leading edge to the total number of genes before the leading edge and the % of genes from the regulon after the leading edge to the total number of genes after the leading edge. This step identified 103 TFs as candidate MRs with *P*-value <0.01. Finally, shadow analysis identified and removed possible false positives. If the regulon of two TFs overlap significantly and only one of them is a MR, then the other may also appear as a MR because of common target enrichment, and the shadow analysis identifies all such MRs. After shadow analysis, we identified 65 master regulators out of which 22 were activated in GC B cells, and 43 inactivated.

Gene Set Enrichment Analysis (GSEA), including *P*-value, normalized enrichment score and false discovery rate, was performed using the GSEA software tool publicly available at the Broad Institute website, as previously described[33]. We used the default parameters, except for the following: geneset permutations (1000 permutations), and the data set was collapsed to gene names (maximum of probes).

Expression heat maps were generated using the MultiExperiment Viewer (MeV v4.8), which is part of the TM4 Microarray Software Suite 59. HG-U133 Plus 2.0 (Affymetrix) expression data from normal B-cell subsets available from Gene Expression Omnibus

(GSE12195) were collapsed to gene names (maximum of probes), and then normalized to Z values using the 'standardize' function of Excel before building the heatmaps.

Statistics

The statistical methods used to determine *P*-values are indicated in each figure legend. One-way analysis of variance (ANOVA) paired with Tukey multiple comparison tests were performed using MATLAB (version R2010b). Two-tailed T-tests (equal variance) were used to determine statistical significance (*P*-values) in luciferase reporter assay. Spearman's rank correlation coefficient was used to determine the ranked correlation of *MEF2B* and *BCL6* expression in normal and tumor B cells.

Supplementary Material

Refer to Web version on PubMed Central for supplementary material.

ACKNOWLEDGMENTS

We would like to thank A. Grunn, M. Fangazio and M. Vasishtha for help with the sequencing analysis; C. Scuoppo for advice and reagents on the inducible lentiviral vector system; A. Holmes for statistical analysis (ANOVA); A. Zelent (The Institute of Cancer Research, London) for the HDAC9 antibody; E. Yeh (MD Anderson) for depositing the Ubc9 plasmid at Addgene; R.T. Hay (University of Dundee) for HA-SUMO1 expression plasmid; and the Flow Cytometry facility of the Herbert Irving Comprehensive Cancer Center. This work was supported by NIH grants PO1-CA092625 and RO1-CA37295 (to R.D.-F) and by a Specialized Center of Research grant from the Leukemia and Lymphoma Society (to R.D.-F). D.D.S. is supported by 5K99 CA151827. KB is supported by the Stewart Trust. L.P. is on leave from the University of Perugia Medical School, Perugia, Italy.

REFERENCES

1. Swerdlow, SH., et al. WHO Classification of Tumours of Haematopoietic and Lymphoid Tissues. Lyon: International Agency for Research on Cancer (IARC); 2008.
2. Alizadeh AA, et al. Distinct types of diffuse large B-cell lymphoma identified by gene expression profiling. Nature. 2000; 403:503–511. [PubMed: 10676951]
3. Lenz G, Staudt LM. Aggressive lymphomas. N Engl J Med. 2010; 362:1417–1429. [PubMed: 20393178]
4. Pasqualucci L, et al. Analysis of the coding genome of diffuse large B-cell lymphoma. Nat Genet. 2011; 43:830–837. [PubMed: 21804550]
5. Morin RD, et al. Frequent mutation of histone-modifying genes in non-Hodgkin lymphoma. Nature. 2011; 476:298–303. [PubMed: 21796119]
6. Lohr JG, et al. Discovery and prioritization of somatic mutations in diffuse large B-cell lymphoma (DLBCL) by whole-exome sequencing. Proc Natl Acad Sci U S A. 2012; 109:3879–3884. [PubMed: 22343534]
7. Zhang J, et al. Genetic heterogeneity of diffuse large B-cell lymphoma. Proc Natl Acad Sci U S A. 2013; 110:1398–1403. [PubMed: 23292937]
8. Pasqualucci L, et al. Inactivating mutations of acetyltransferase genes in B-cell lymphoma. Nature. 2011; 471:189–195. [PubMed: 21390126]
9. Challa-Malladi M, et al. Combined genetic inactivation of beta2-Microglobulin and CD58 reveals frequent escape from immune recognition in diffuse large B cell lymphoma. Cancer Cell. 2011; 20:728–740. [PubMed: 22137796]
10. Iqbal J, et al. Distinctive patterns of BCL6 molecular alterations and their functional consequences in different subgroups of diffuse large B-cell lymphoma. Leukemia. 2007; 21:2332–2343. [PubMed: 17625604]

11. Pasqualucci L. The genetic basis of diffuse large B-cell lymphoma. Current opinion in hematology. 2013; 20:336–344. [PubMed: 23673341]
12. Morin RD, et al. Somatic mutations altering EZH2 (Tyr641) in follicular and diffuse large B-cell lymphomas of germinal-center origin. Nat Genet. 2010; 42:181–185. [PubMed: 20081860]
13. Compagno M, et al. Mutations of multiple genes cause deregulation of NF-kappaB in diffuse large B-cell lymphoma. Nature. 2009; 459:717–721. [PubMed: 19412164]
14. Pasqualucci L, et al. Inactivation of the PRDM1/BLIMP1 gene in diffuse large B cell lymphoma. J Exp Med. 2006; 203:311–317. [PubMed: 16492805]
15. Tam W, et al. Mutational analysis of PRDM1 indicates a tumor-suppressor role in diffuse large B-cell lymphomas. Blood. 2006; 107:4090–4100. [PubMed: 16424392]
16. Pasqualucci L, et al. Mutations of the BCL6 proto-oncogene disrupt its negative autoregulation in diffuse large B-cell lymphoma. Blood. 2003; 101:2914–2923. [PubMed: 12515714]
17. Potthoff MJ, Olson EN. MEF2: a central regulator of diverse developmental programs. Development. 2007; 134:4131–4140. [PubMed: 17959722]
18. Molkentin JD, et al. MEF2B is a potent transactivator expressed in early myogenic lineages. Mol Cell Biol. 1996; 16:3814–3824. [PubMed: 8668199]
19. Gossett LA, Kelvin DJ, Sternberg EA, Olson EN. A new myocyte-specific enhancer-binding factor that recognizes a conserved element associated with multiple muscle-specific genes. Mol Cell Biol. 1989; 9:5022–5033. [PubMed: 2601707]
20. Han A, et al. Sequence-specific recruitment of transcriptional co-repressor Cabin1 by myocyte enhancer factor-2. Nature. 2003; 422:730–734. [PubMed: 12700764]
21. Youn HD, Sun L, Prywes R, Liu JO. Apoptosis of T cells mediated by Ca2+-induced release of the transcription factor MEF2. Science. 1999; 286:790–793. [PubMed: 10531067]
22. Youn HD, Liu JO. Cabin1 represses MEF2-dependent Nur77 expression and T cell apoptosis by controlling association of histone deacetylases and acetylases with MEF2. Immunity. 2000; 13:85–94. [PubMed: 10933397]
23. Khiem D, Cyster JG, Schwarz JJ, Black BL. A p38 MAPK-MEF2C pathway regulates B-cell proliferation. Proc Natl Acad Sci U S A. 2008; 105:17067–17072. [PubMed: 18955699]
24. Wilker PR, et al. Transcription factor Mef2c is required for B cell proliferation and survival after antigen receptor stimulation. Nat Immunol. 2008; 9:603–612. [PubMed: 18438409]
25. Klein U, et al. Transcriptional analysis of the B cell germinal center reaction. Proc Natl Acad Sci U S A. 2003; 100:2639–2644. [PubMed: 12604779]
26. Basso K, Dalla-Favera R. Roles of BCL6 in normal and transformed germinal center B cells. Immunol Rev. 2012; 247:172–183. [PubMed: 22500840]
27. Cattoretti G, et al. BCL-6 protein is expressed in germinal-center B cells. Blood. 1995; 86:45–53. [PubMed: 7795255]
28. Lefebvre C, et al. A human B-cell interactome identifies MYB and FOXM1 as master regulators of proliferation in germinal centers. Mol Syst Biol. 2010; 6:377. [PubMed: 20531406]
29. Krzywinski M, et al. Circos: an information aesthetic for comparative genomics. Genome Res. 2009; 19:1639–1645. [PubMed: 19541911]
30. Basso K, et al. Reverse engineering of regulatory networks in human B cells. Nat Genet. 2005; 37:382–390. [PubMed: 15778709]
31. Basso K, et al. Integrated biochemical and computational approach identifies BCL6 direct target genes controlling multiple pathways in normal germinal center B cells. Blood. 2010; 115:975–984. [PubMed: 19965633]
32. Meerbrey KL, et al. The pINDUCER lentiviral toolkit for inducible RNA interference in vitro and in vivo. Proc Natl Acad Sci U S A. 2011; 108:3665–3670. [PubMed: 21307310]
33. Subramanian A, et al. Gene set enrichment analysis: a knowledge-based approach for interpreting genome-wide expression profiles. Proc Natl Acad Sci U S A. 2005; 102:15545–15550. [PubMed: 16199517]
34. Du M, et al. Protein kinase A represses skeletal myogenesis by targeting myocyte enhancer factor 2D. Mol Cell Biol. 2008; 28:2952–2970. [PubMed: 18299387]

35. Skalhegg BS, Tasken K. Specificity in the cAMP/PKA signaling pathway. Differential expression,regulation, and subcellular localization of subunits of PKA. Frontiers in bioscience : a journal and virtual library. 2000; 5:D678–D693. [PubMed: 10922298]
36. Seamon K, Daly JW. Activation of adenylate cyclase by the diterpene forskolin does not require the guanine nucleotide regulatory protein. J Biol Chem. 1981; 256:9799–9801. [PubMed: 6268630]
37. Chijiwa T, et al. Inhibition of forskolin-induced neurite outgrowth and protein phosphorylation by a newly synthesized selective inhibitor of cyclic AMP-dependent protein kinase, N-[2-(p-bromocinnamylamino)ethyl]-5-isoquinolinesulfonamide (H-89), of PC12D pheochromocytoma cells. J Biol Chem. 1990; 265:5267–5272. [PubMed: 2156866]
38. Iyer GH, Moore MJ, Taylor SS. Consequences of lysine 72 mutation on the phosphorylation and activation state of cAMP-dependent kinase. J Biol Chem. 2005; 280:8800–8807. [PubMed: 15618230]
39. Hietakangas V, et al. PDSM, a motif for phosphorylation-dependent SUMO modification. Proceedings of the National Academy of Sciences of the United States of America. 2006; 103:45–50. [PubMed: 16371476]
40. Mohideen F, et al. A molecular basis for phosphorylation-dependent SUMO conjugation by the E2 UBC9. Nat Struct Mol Biol. 2009; 16:945–952. [PubMed: 19684601]
41. Gregoire S, et al. Control of MEF2 transcriptional activity by coordinated phosphorylation and sumoylation. J Biol Chem. 2006; 281:4423–4433. [PubMed: 16356933]
42. Kang J, Gocke CB, Yu H. Phosphorylation-facilitated sumoylation of MEF2C negatively regulates its transcriptional activity. BMC biochemistry. 2006; 7:5. [PubMed: 16478538]
43. Molkentin JD, Black BL, Martin JF, Olson EN. Cooperative activation of muscle gene expression by MEF2 and myogenic bHLH proteins. Cell. 1995; 83:1125–1136. [PubMed: 8548800]
44. Pasqualucci L, Kitaura Y, Gu H, Dalla-Favera R. PKA-mediated phosphorylation regulates the function of activation-induced deaminase (AID) in B cells. Proc Natl Acad Sci U S A. 2006; 103:395–400. [PubMed: 16387847]
45. Basu U, et al. The AID antibody diversification enzyme is regulated by protein kinase A phosphorylation. Nature. 2005; 438:508–511. [PubMed: 16251902]
46. Baron BW, et al. Identification of the gene associated with the recurring chromosomal translocations t(3;14)(q27;q32) and t(3;22)(q27;q11) in B-cell lymphomas. Proc Natl Acad Sci U S A. 1993; 90:5262–5266. [PubMed: 8506375]
47. Ye BH, Rao PH, Chaganti RS, Dalla-Favera R. Cloning of bcl-6, the locus involved in chromosome translocations affecting band 3q27 in B-cell lymphoma. Cancer Res. 1993; 53:2732–2735. [PubMed: 8504412]
48. Cattoretti G, et al. Deregulated BCL6 expression recapitulates the pathogenesis of human diffuse large B cell lymphomas in mice. Cancer Cell. 2005; 7:445–455. [PubMed: 15894265]
49. Ye BH, et al. Chromosomal translocations cause deregulated BCL6 expression by promoter substitution in B cell lymphoma. Embo J. 1995; 14:6209–6217. [PubMed: 8557040]
50. Duan S, et al. FBXO11 targets BCL6 for degradation and is inactivated in diffuse large B-cell lymphomas. Nature. 2012; 481:90–93. [PubMed: 22113614]
51. Cerchietti LC, et al. A small-molecule inhibitor of BCL6 kills DLBCL cells in vitro and in vivo. Cancer Cell. 2010; 17:400–411. [PubMed: 20385364]
52. Bieber T, Elsasser HP. Preparation of a low molecular weight polyethylenimine for efficient cell transfection. Biotechniques. 2001; 30:74–77. 80-1. [PubMed: 11196323]
53. Fellmann C, et al. Functional identification of optimized RNAi triggers using a massively parallel sensor assay. Molecular cell. 2011; 41:733–746. [PubMed: 21353615]
54. Scuoppo C, et al. A tumour suppressor network relying on the polyamine-hypusine axis. Nature. 2012; 487:244–248. [PubMed: 22722845]
55. Dominguez-Sola D, et al. Non-transcriptional control of DNA replication by c-Myc. Nature. 2007; 448:445–451. [PubMed: 17597761]
56. Dominguez-Sola D, et al. The proto-oncogene MYC is required for selection in the germinal center and cyclic reentry. Nature immunology. 2012; 13:1083–1091. [PubMed: 23001145]

57. Margolin AA, et al. ARACNE: an algorithm for the reconstruction of gene regulatory networks in a mammalian cellular context. BMC Bioinformatics. 2006; 1(7 Suppl):S7. [PubMed: 16723010]

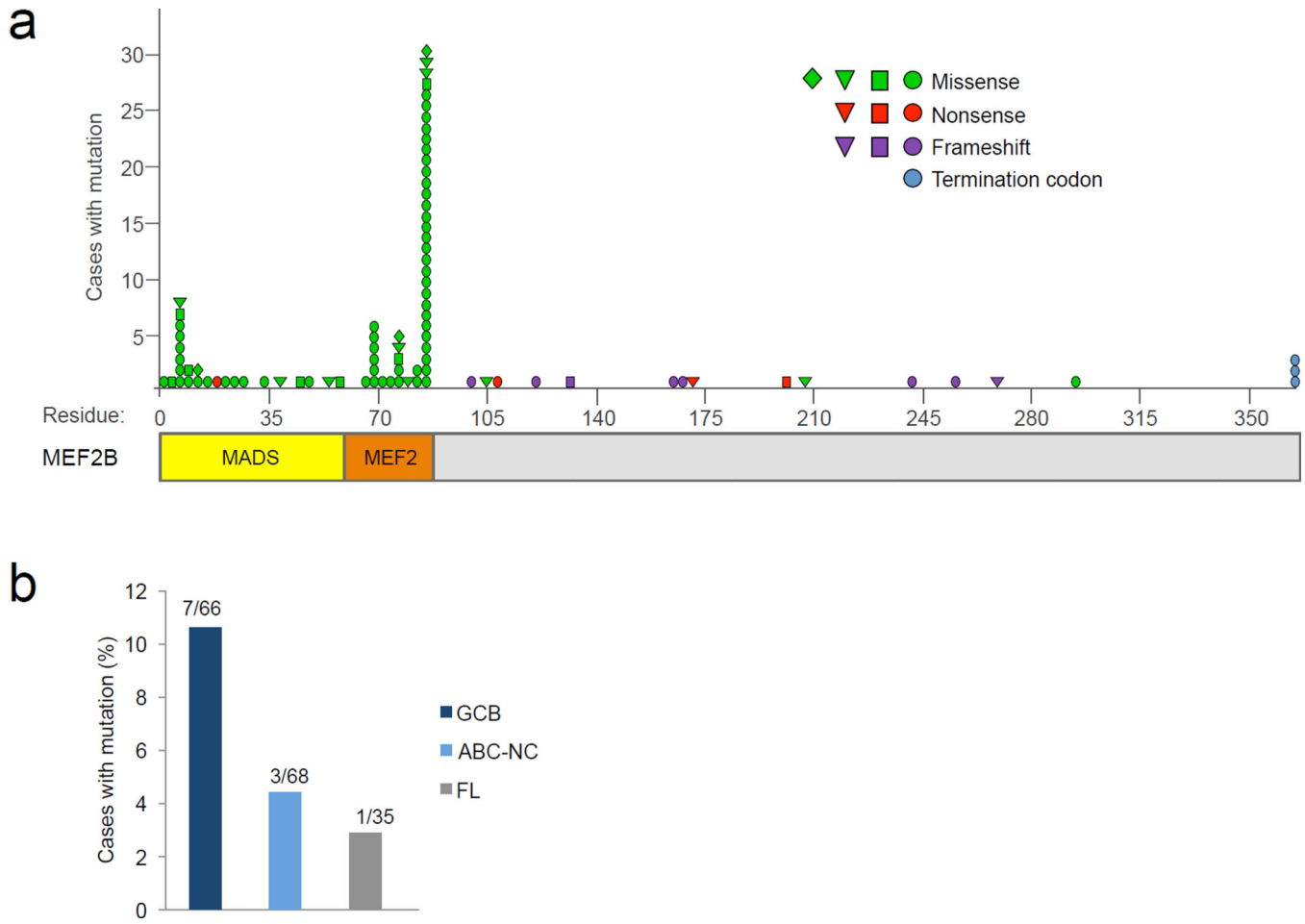

Figure 1. *MEF2B* is targeted predominantly by missense mutations in DLBCL and FL

(**a**) Schematic representation of the MEF2B protein (bottom) with the MADS-box (yellow) and the MEF2 domain (orange). Distribution of missense (green), nonsense (red), frameshift (purple) and termination codon (blue) mutations detected in DLBCL and FL cases; geometric shapes distinguish *MEF2B* mutations reported in our study[4] (triangles); Lohr et al., 2012[6] (squares); Morin et al., 2011[5] (circles); and Zhang et al., 2013[7] (diamonds). Only mutations not reported in SNP databases were considered. (**b**) Distribution of *MEF2B* mutations in GCB- and ABC-NC-DLBCL and in FL in our dataset; the number of mutated samples over total samples analyzed is shown (n=169; NC, non-classified).

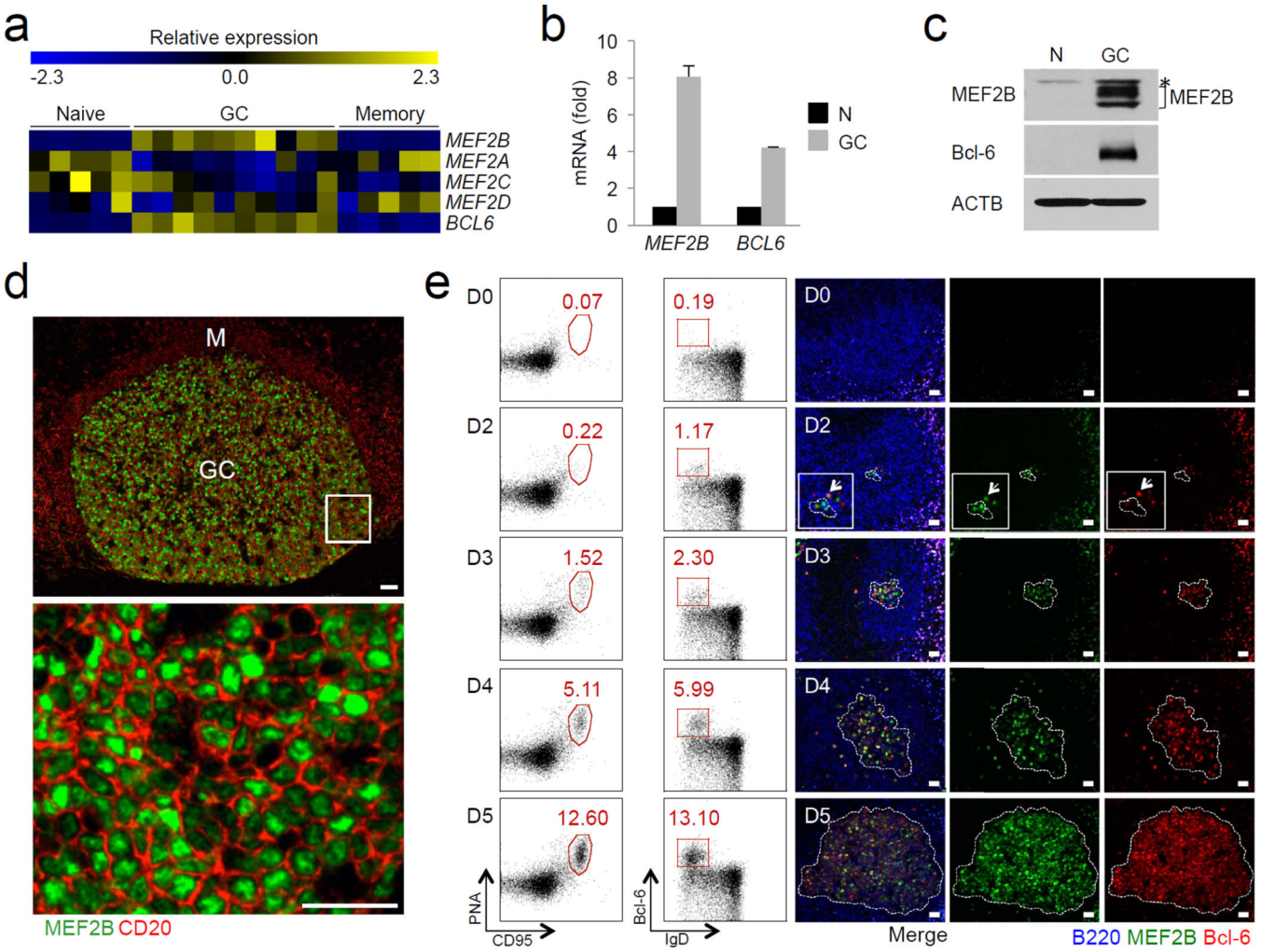

Figure 2. MEF2B is expressed in GC B cells

(**a**) Gene expression profiles of *MEF2* family members and *BCL6* in normal mature B cell subpopulations (GeneChIP® Human Genome U133 Plus 2.0, Affymetrix). Each column corresponds to an independent sample of naive, GC or memory B cells. Scale bar represents the relative expression (Z value) across samples. (**b**) qRT-PCR analysis of *MEF2B* and *BCL6* mRNA in naive (N) and GC B cells from human tonsils (mean ± SD of three technical replicates). (**c**) Immunoblot analysis of MEF2B, Bcl-6 and ACTB in N and GC B cells. Asterisk, non-specific band. (**d**) Double immunofluorescence staining of MEF2B (green) and CD20 (red) in human tonsil section (GC, germinal center; M, mantle zone). Below, higher magnification of inset. Scale bars, 20 μm. (**e**) Kinetics of MEF2B and Bcl-6 protein expression during the GC reaction. Dot plots (left) highlight pools of GC-committed B cells ($PNA^{hi}CD95^{hi}$), and appearance of Bcl-6 expression ($Bcl\text{-}6^{hi}$, IgD^{lo}) in mouse splenic B cells. Percentage of GC B cells within the total B cell compartment are indicated. Right, MEF2B and BCL6 immunofluorescence analysis in B cell clusters of splenic white pulp in the same samples as in the dot plots. Dashed white outlines circle GC B cell clusters. Arrow in the D2 (day 2) inset highlights a B cell with Bcl-6 and MEF2B co-expression, while most cells in this early pre-GC cluster are positive for MEF2B but show low or absent Bcl-6

expression. Scale bars, 25 μm. Representative of 2 independent experiments; 1 mouse per timepoint.

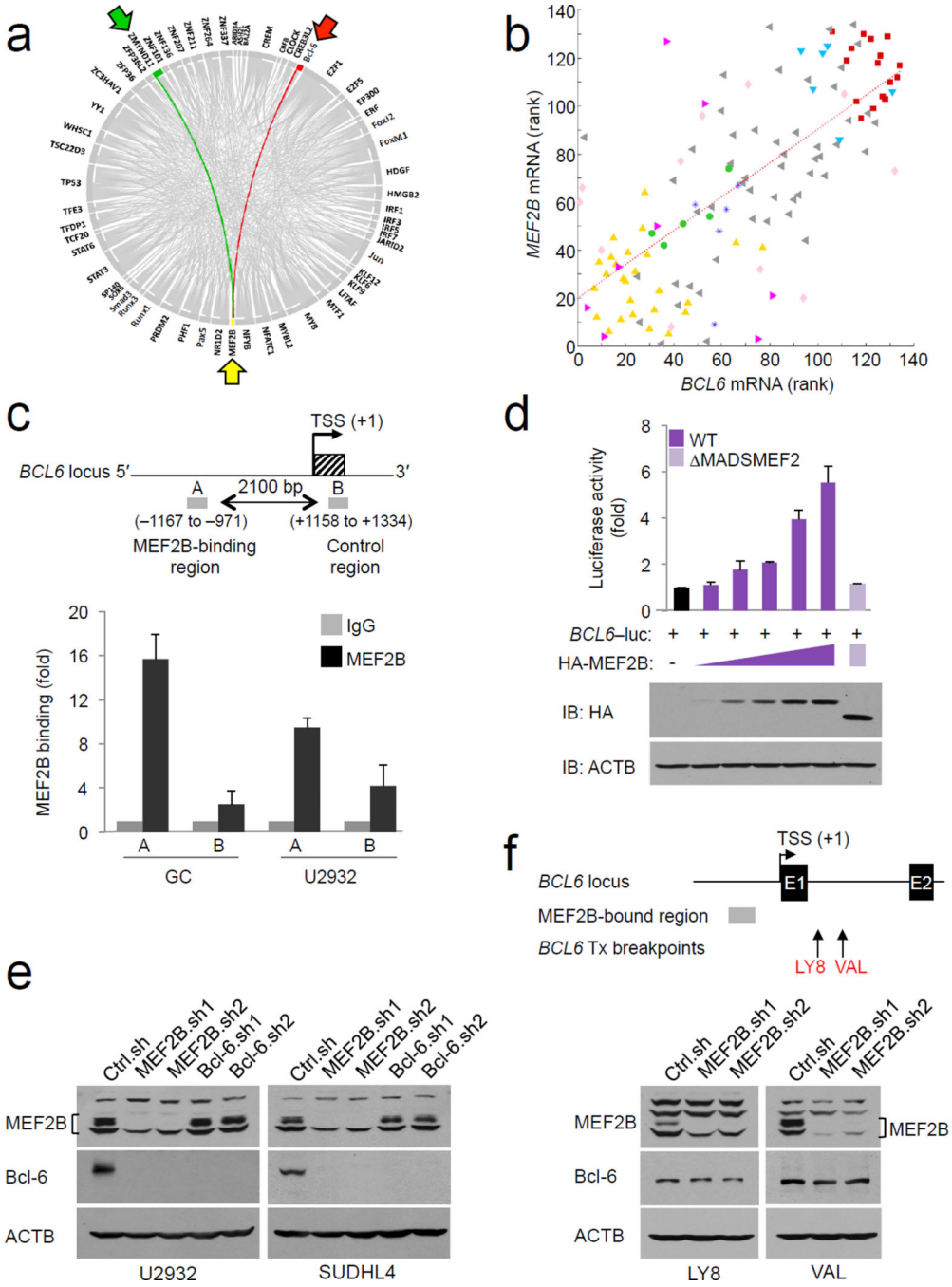

Figure 3. *BCL6* is a direct transcriptional target of MEF2B in GC B cells

(**a**) Circos plot representing connections between transcription factors identified as GC master regulators as predicted by the ARACNe algorithm[30]. MEF2B (yellow arrow) is only linked to Bcl-6 (red arrow) and ZMYND11 (green arrow). Red and green lines denote positive and negative correlation, respectively. (**b**) Ranked correlation between *MEF2B* and *BCL6* expression in normal B cells (red, GC (n = 16); dark blue, naive (n = 5); green, memory (n = 5)) and tumor cells (yellow, Chronic Lymphocytic Leukemia (n = 26); dark pink, Mantle Cell Lymphoma (n = 8); light blue, FL (n = 6); light pink, Burkitt Lymphoma

(n = 11); grey, DLBCL (n = 51)). (Spearman's rank correlation coefficient, $R^2 = 0.7$). (**c**) Top, schematic representation of the *BCL6* promoter; (TSS, transcription start site). Location of MEF2B-binding region (A) and control region (B) is indicated relative to the TSS. Bottom, analysis of MEF2B binding to the *BCL6* promoter by quantitative PCR on ChIP DNA (mean ± SD of three technical replicates). (**d**) Top, Reporter assay using the native *BCL6* promoter region (−1593/−672, *BCL6*-luc), co-transfected with HA-MEF2B or a transcription defective mutant (HA-MEF2BΔMADSMEF2) into HEK293T cells (mean ±SD, n=4). Bottom, immunoblot analysis on same lysates. (**e**) Immunoblot analysis of MEF2B, Bcl-6, and ACTB in U2932 and SUDHL4 cell lines, transduced with lentiviral vectors expressing control shRNA (Ctrl.sh), two different MEF2B- or Bcl-6-targeting shRNAs. Representative results of two independent experiments. (**f**) Top, schematic representation of the *BCL6* locus with the MEF2B-bound region (grey box), and arrows pointing to translocation breakpoints in LY8 and VAL DLBCL cell lines. Bottom, immunoblot analysis of MEF2B, Bcl-6 and ACTB in LY8 and VAL cell lines, transduced with lentiviral vectors expressing the indicated shRNAs. Results are representative of two independent experiments.

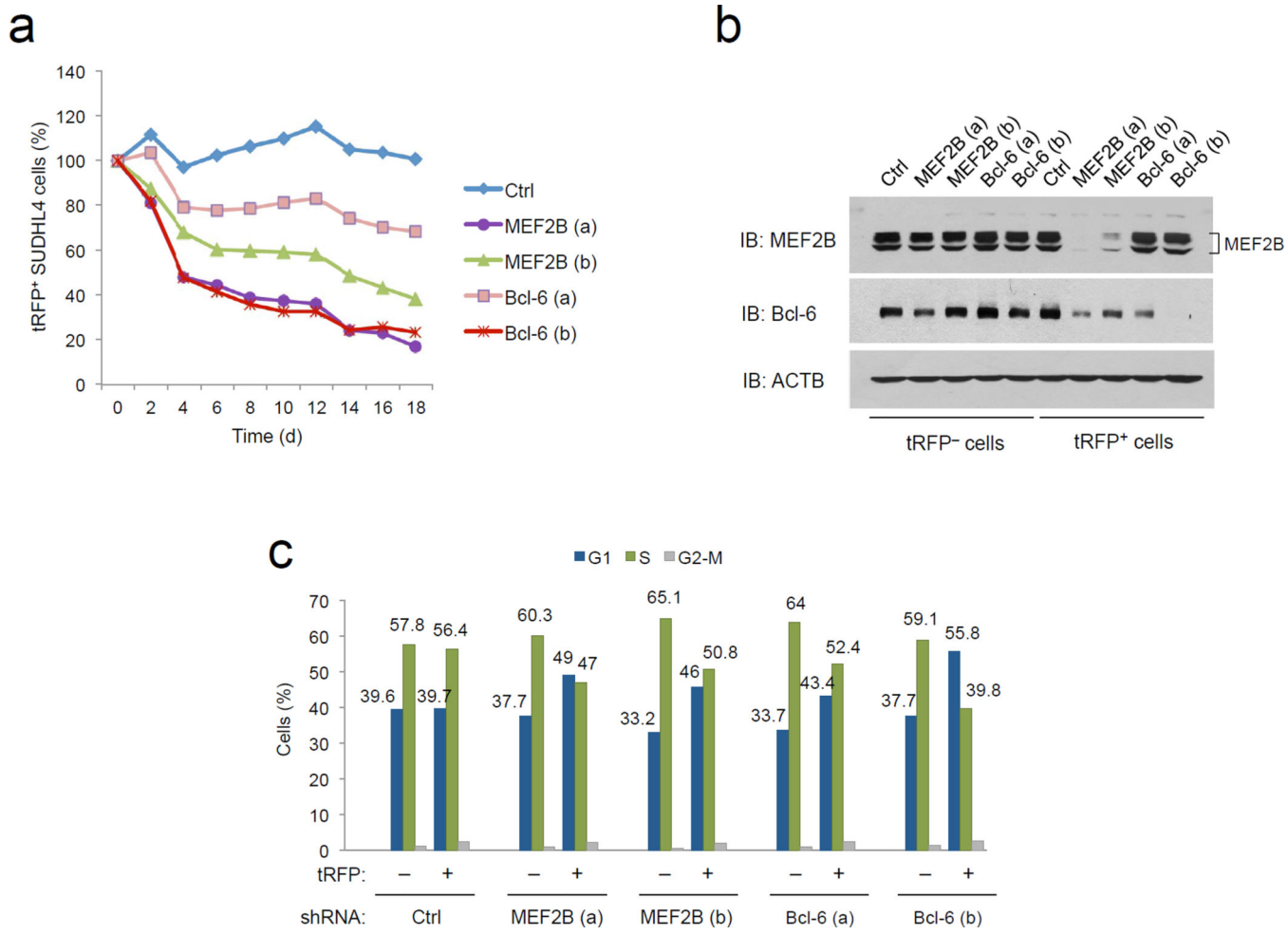

Figure 4. MEF2B is required for cell cycle progression and proliferation in DLBCL

(**a**) Time course of tRFP$^+$ SUDHL4 cells infected with inducible lentiviral vectors expressing control (Ctrl), two different MEF2B- or Bcl-6-targeting shRNAs and co-cultured with uninfected cells (1:1 ratio). The number of cells at time t=0 set as 100%. Induction of shRNA expression was achieved and maintained by adding Doxycycline in the cultures for a period of 18 days. (**b**) Immunoblot analysis of MEF2B, Bcl-6 and ACTB proteins in tRFP$^+$ and tRFP$^-$ SUDHL4 cells at day 2 of co-culture. (**c**) Cell cycle profiles of tRFP$^+$ and tRFP$^-$ cell populations at day 2 of co-culture. Percentages of cells in G1, S, and G2-M detected by BrdU and 7-AAD staining are indicated in the bar graph. Specific phase gates used for quantitation are shown in Supplementary Fig. 4d,e. Results (**a–c**) are representative of two independent experiments; one cell pool per hairpin.

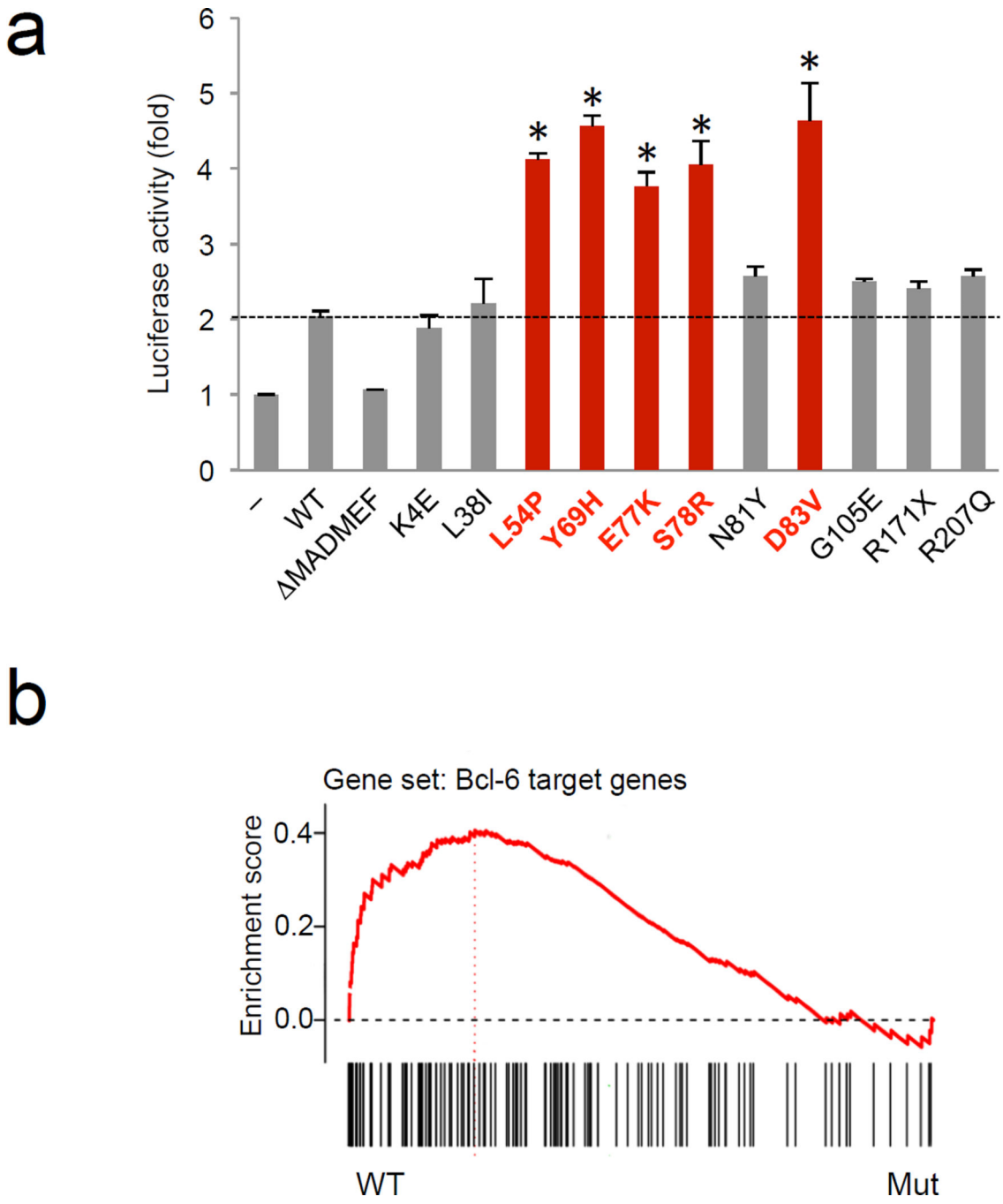

Figure 5. N-terminal MEF2B mutations enhance *BCL6* transcription and correlate with increased Bcl-6 biological activity in DLBCL primary cases

(**a**) Reporter assay in HEK293T cells using a *BCL6* reporter construct driven by the native *BCL6* promoter region (−1593/−672, encompassing MEF2B-bound region), together with expression vectors encoding for wild-type or mutant HA-MEF2B alleles. The dotted line indicates wild-type HA-MEF2B activity. MEF2B mutants depicted with red bars have significantly increased transcriptional activity as compared to wild-type MEF2B (asterisk: $P < 0.05$, one-way ANOVA paired with Tukey multiple comparison test). Results are

representative of three independent experiments, with two technical replicates in each experiment. (**b**) GSEA plot illustrating the enrichment of the Bcl-6 'core transcriptional signature'[31] in DLBCL primary cases with wild-type MEF2B (WT; $n = 8$) versus DLBCL primary cases with mutant MEF2B displaying increased transcriptional activity on the *BCL6* promoter (Mut; $n = 3$; cases carrying L54P, E77K, S78R mutations). P-value < 0.00001; False discovery rate, FDR < 0.00001; Normalized enrichment score, NES = 2.05.

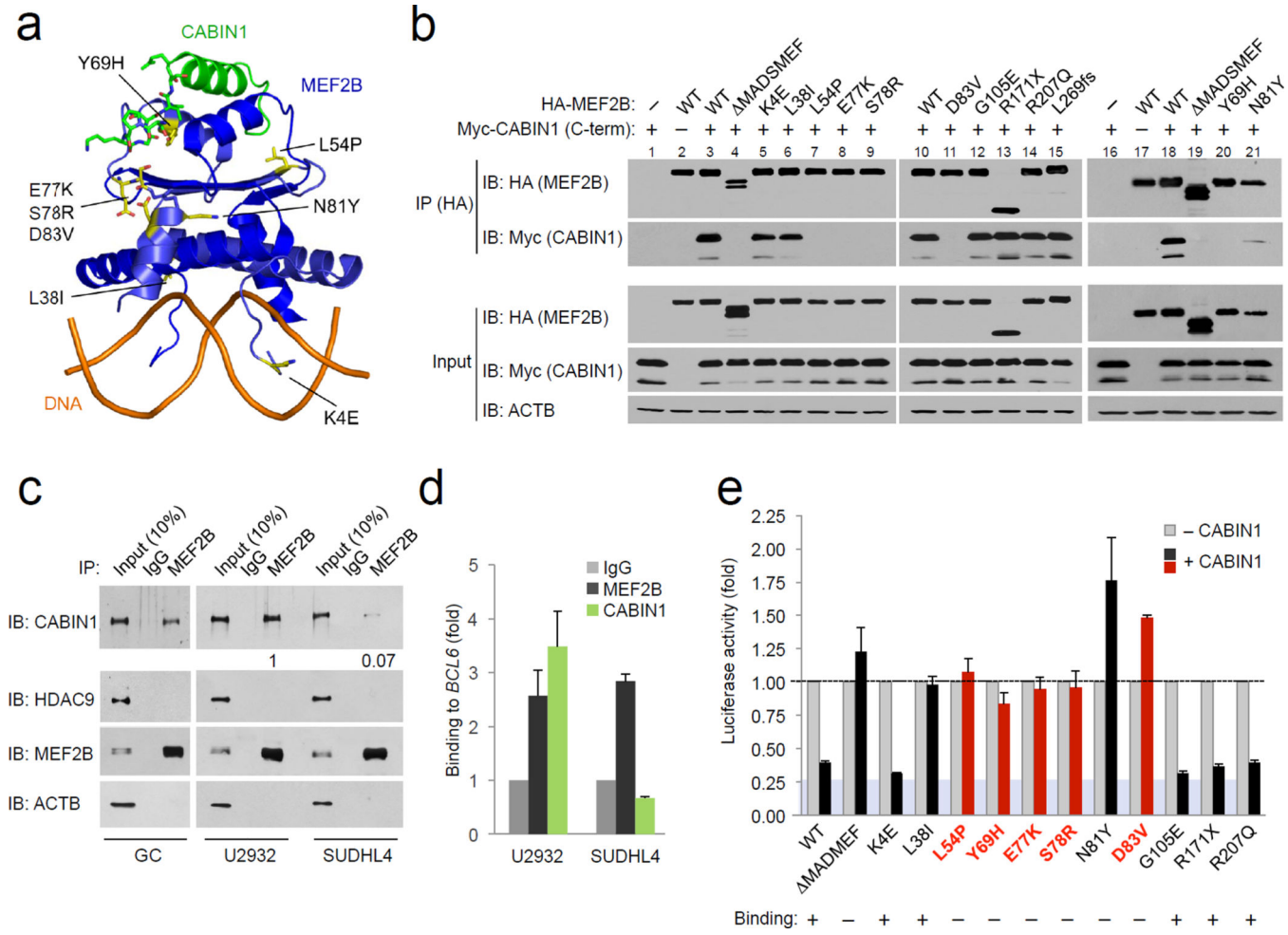

Figure 6. MEF2B N-terminus mutants fail to bind CABIN1 and escape its co-repressor activity

(**a**) Crystal structure of MEF2B (blue) in complex with DNA (orange) and the CABIN1 co-repressor (green)[20]. Residues mutated in DLBCL or FL are in yellow and shown as a stick model. (**b**) HA immunoprecipitates from HEK293T cells co-transfected with expression vectors encoding wild-type or mutant HA-MEF2B alleles, and Myc-tagged CABIN1 (residues 2037–2220). Lanes 1–15 and lanes 16–21 are from two separate experiments. Results are representative of three independent experiments. (**c**) Co-immunoprecipitation assay in nuclear extracts from GC B cells or from cell lines, U2932 (*MEF2B* wild-type) and SUDHL4 (*MEF2B* D83V, heterozygous). Nuclear extracts were immunoprecipitated with anti-MEF2B or anti-IgG, and analyzed by immunoblotting. Relative amounts of CABIN1 in MEF2B immunoprecipitates were quantitated by densitometry and indicated below. Results are representative of two independent experiments. (**d**) Quantitative PCR for MEF2B-bound region in the *BCL6* promoter using MEF2B or CABIN1 ChIP DNA (mean ± SD of three technical replicates) from U2932 and SUDHL4 cells. (**e**) Reporter assay using a construct driven by the native *BCL6* promoter region co-transfected with vectors encoding wild-type or mutant HA-MEF2B alleles in the presence or absence of Myc-tagged CABIN1 (residues 2037–2220). Results are displayed as relative luciferase activity in the presence of CABIN1 (black and red bars), compared to the activity in its absence (grey bars) (set at 1, dotted line)

(mean ±SD; n = 2 biological replicates). Red bars highlight MEF2B mutants with enhanced transcriptional activity on the *BCL6* promoter (see Fig. 5a). Shaded background indicates basal reporter activity in absence of MEF2B.

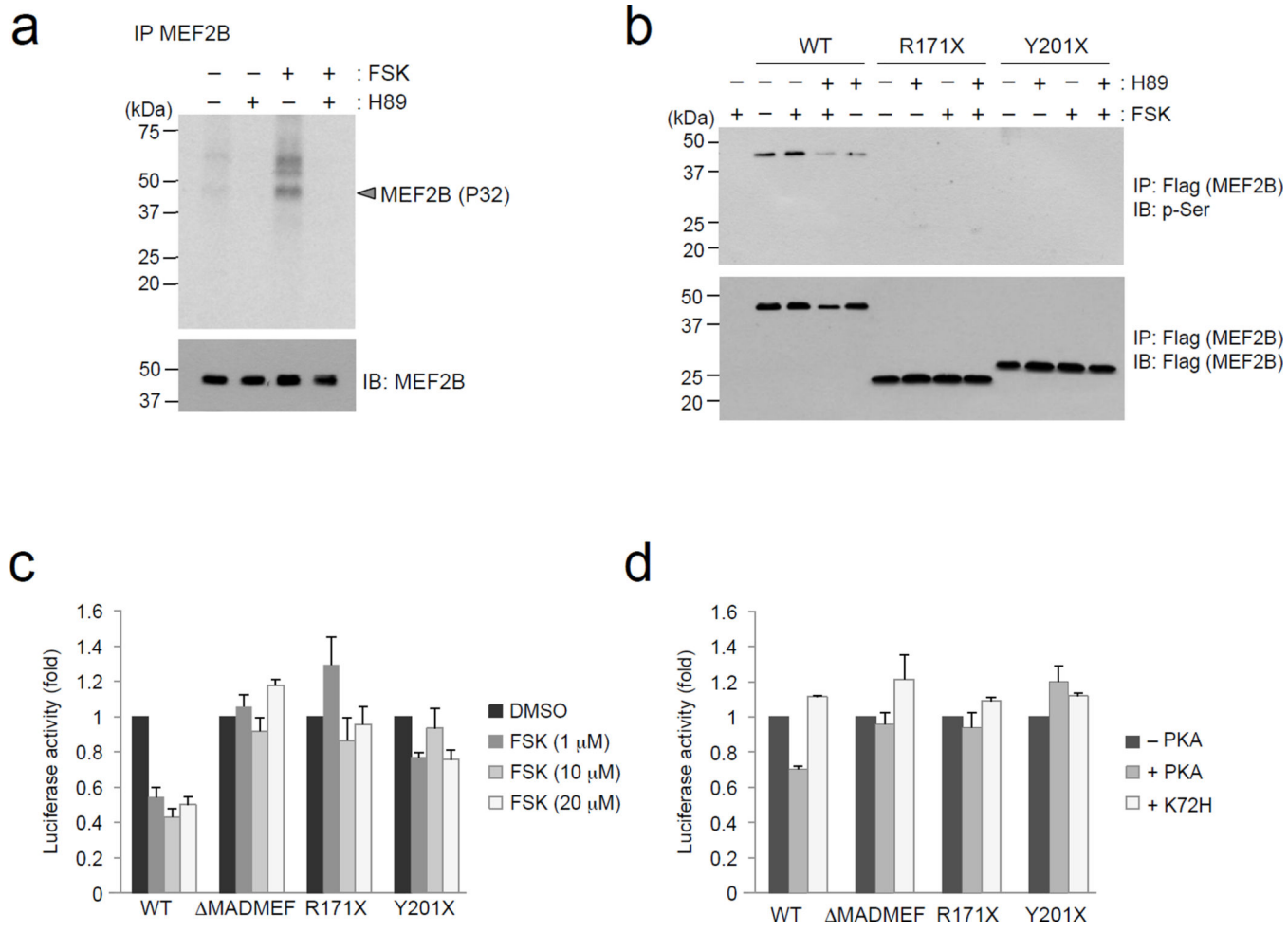

Figure 7. C-terminal truncated MEF2B proteins escape negative regulation by PKA-dependent phosphorylation

(**a**) *In vivo* metabolic labeling with ^{32}P orthophosphate of SUDHL4 DLBCL cells, incubated in presence or absence of Forskolin (FSK) and/or H89, as indicated. Endogenous MEF2B immunoprecipitates were resolved by SDS-PAGE: top, gel exposed to autoradiography film; bottom, immunoblot analysis of MEF2B in the same samples. Results are representative of two independent experiments. (**b**) Flag-tagged MEF2B alleles (WT, R171X and Y201X) were transfected in HEK293T cells. Cells were harvested upon treatment with FSK and/or H89, and Flag immunoprecipitates were eluted, resolved by SDS-PAGE, and immunoblotted with the indicated antibodies. Results are representative of two independent experiments. (**c**) Luciferase reporter assay using a construct driven by the native *BCL6* promoter, co-transfected with HA-tagged MEF2B (wild-type and mutants) in HEK293T cells. Cells were treated with DMSO or FSK overnight before harvesting. Results are displayed as relative luciferase activity (MEF2B+DMSO set at 1), normalized to Renilla luciferase activity (mean ±SD; n = 2 biological replicates). (**d**) Luciferase reporter assay using a construct driven by the native *BCL6* promoter co-transfected with expression vectors encoding HA-tagged MEF2B (wild-type or mutants) in the presence or absence of an expression vector encoding for PKA (wild-type or kinase dead mutant, K72H) in HEK293T cells. Results are displayed as relative luciferase activity in the presence of PKA, compared

to the activity in its absence (set at 1), and normalized to Renilla luciferase activity. Results are representative of three independent experiments (two technical replicates in each experiment).

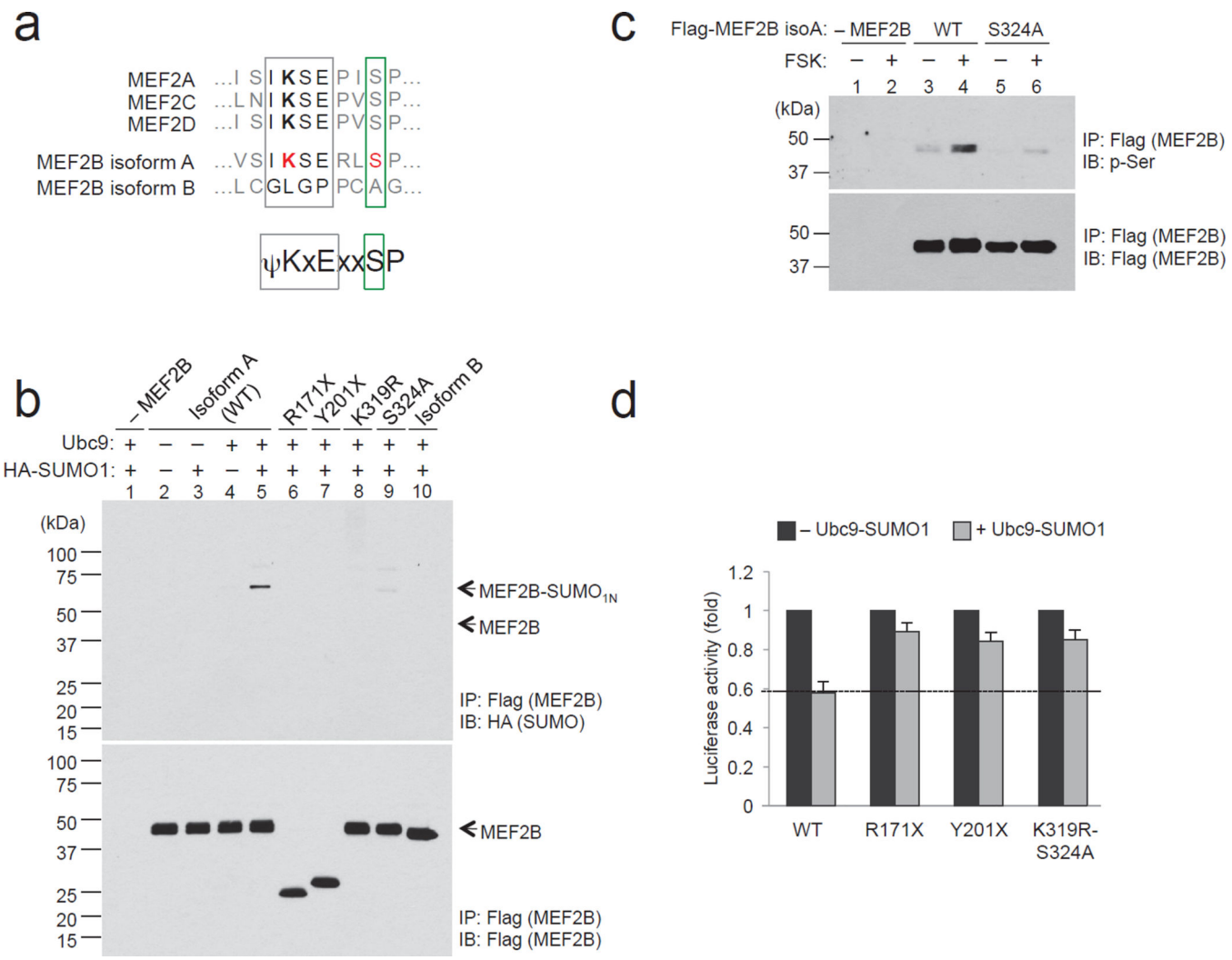

Figure 8. C-terminal mutations abrogate negative regulation of MEF2B by phosphorylation-dependent sumoylation

(**a**) Sequence alignment of the conserved phosphorylation-dependent sumoylation motif (PDSM, ψKxExxSP), found in the C-terminus of human MEF2A, MEF2C, MEF2D and MEF2B isoform A. PDSM is composed of a sumoylation consensus site (grey box) and a proline-directed phosphorylation site (green box). The K319 and S324 residues of the MEF2B PDSM are highlighted in red. (**b**) *In vivo* sumoylation assay in HEK293T cells, co-transfected with expression vectors encoding for Flag-tagged MEF2B isoform A (wild-type and mutants) and isoform B, Ubc9 and HA-tagged SUMO1. Flag immunoprecipitates were analyzed by immunoblotting using anti-HA and anti-Flag. Top, monosumoylated MEF2B; bottom, unmodified MEF2B protein. Results are representative of two independent experiments. (**c**) HEK293T cells were transfected with expression vectors encoding Flag-tagged MEF2B (wild-type or S324A mutant), and incubated in the presence or absence of Forskolin (FSK), as indicated. Flag immunoprecipitates were analyzed by immunoblotting using anti-phospho-serine and anti-Flag. (**d**) Luciferase reporter assay using a construct driven by the native *BCL6* promoter region, co-transfected with expression vectors encoding Ubc9, SUMO1, and MEF2B (wild-type; C-terminal truncating mutations, R171X and

Y201X; or selected mutations in the PDSM consensus site: K319R–S324A) in HEK293T cells. Results are displayed as relative luciferase activity (mean ±SD; n = 2 biological replicates).